November 2017

Electrical, Optical and Thermal Investigations of Cobalt Oxide-Antimony Doped Tin Oxide (CoO-ATO) Thin Films and Nanofiber Membranes

Nirmita Roy
University of South Florida, nirmitaroy@mail.usf.edu

Electrical, Optical and Thermal Investigations of Cobalt Oxide-Antimony Doped Tin Oxide (CoO-ATO) Thin Films and Nanofiber Membranes

by

Nirmita Roy

A thesis submitted in partial fulfillment
of the requirements for the degree of
Master of Science in Electrical Engineering
Department of Electrical Engineering
College of Engineering
University of South Florida

Major Professor: Sylvia Thomas, Ph.D.
Andrew Hoff, Ph.D.
Arash Takshi, Ph.D.

Date of Approval:
October 26, 2017

Keywords: Solar cell, Electro spinning, Spin coating,
UV-VIS, FTIR, Thermal impact

DEDICATION

My thesis is dedicated to my parents, brother and sister-in-law who have always been my backbone and supported me to accomplish my dreams. I would also like to dedicate this work to my friends who have stood by my side throughout my journey.

ACKNOWLEDGMENTS

A humongous thank you to Dr. Sylvia Thomas and Manopriya Devisetty Subramanyam for supervising me through my project. My sincere gratitude to the AMBIR group for their encouragement, the staff and faculty at NREC, USF for all the equipment trainings.

I would also like to thank all my professors at USF, my family and friends and my committee members for their immense support, without whom all this would have not been possible.

TABLE OF CONTENTS

LIST OF TABLES

LIST OF FIGURES

ABSTRACT

The main aim of this thesis work is to investigate the electrical, optical and thermal impact characteristics of cobalt oxide doped antimony tin oxide (CoO-ATO) in the form of thin films and nanofiber membranes. CoO-ATO is a novel composite material that has the potential to be used as reinforced aircraft coatings, military garment coatings, or more specifically as an anti-reflective (AR) top coating for photovoltaic (PV) cells. This work will be critical in determining the effectiveness of using a CoO-ATO layer in these applications. Electrospun nanofibers and spin coated thin films consisting of a polymeric solution of CoO-ATO will be used. Thin films are created using spin coating techniques, and nanofiber membranes are created using an electrospinning technique. Polystyrene (PS) will be used as a solute, and chloroform as a solvent, to create the solution. It is hypothesized that coatings of this material will have improved optical characteristics as compared to traditional ATO coatings and minimum impact from thermal cycling making it a favorable candidate for PV cells. This work will do an electrical, optical and thermal cycling impact characterization of CoO-ATO thin films and nanofiber membranes for a doping range of x% CoO where x ranged from $0.2<x<2.0$. Thermal cycling will cover a temperature range of 35 degrees to 85 degrees Celsius, which is typically used when fabricating Si solar cells. As work progresses, thin films and nanofiber membranes showing good I-V characteristics after thermal cycling will be used as coatings on 3" x 6" Si solar cells to demonstrate performance.

1 INTRODUCTION

1.1 Background and Motivation

Globally, a comprehensive growth in the advancement of material improvement and applications has been observed in every industry and is in progression even today. The demand to increase material functionality involves characterizing new materials to be utilized in diverse applications. One of the most important factors to continue seeing the growth in the industry is by potentially being able to explain materials based on its compositions, structures, characterizations and applications. Characterizing distinct properties of a material system is critical in determining which materials are suitable to meet certain technology challenges.

The exposure of infrared radiations to many applications or devices is causing damages, and researchers are investigating coatings to prevent or reduce these damages. For example, a collection of material coatings can be added to the aerospace vehicle structures to promote longer life span and stealth of these vehicles. The added coatings when characterized indicated that when infrared light photons were emitted towards the vehicle surface, they would be absorbed or reflected, thus helping to preserve the aircraft structure by making it light weight and easy to maneuver [8-10].

Similarly, these anti-reflective coatings (ARC) can be instrumental in a photovoltaic (PV) cell or a traditional solar cell that transforms the energy from the sun into electricity. Figure 1 shows the schematic operation of a PV cell. It consists of a p-n junction with a very thin and heavily doped n-region, where the illumination takes place. An external circuit is connected to

generate electricity. The depletion region with a built-in field E_0 is primarily extending into the p-side of the cell. The n-region has electrodes attached and the light enters the device and produces a small series resistance.

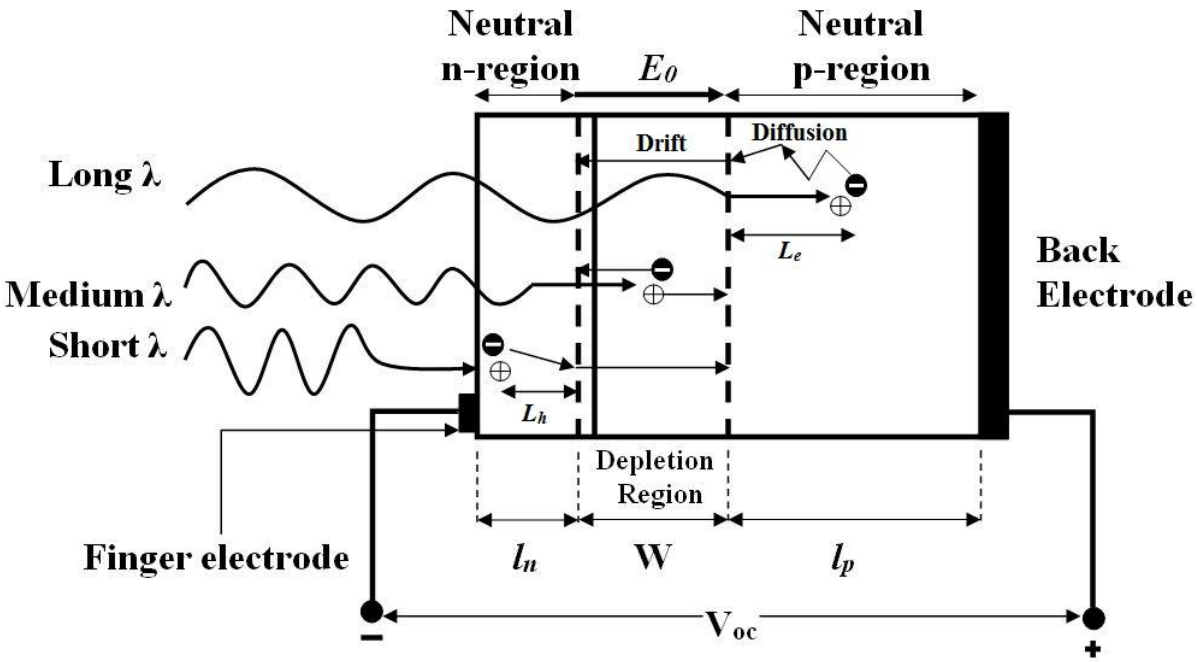

Figure 1: Principle of operation of a solar cell [25]

When the light is incident on the solar cell, most of the photons are absorbed in the n-region, and the photons induce electron-hole pairs (EHP). There is an external load connected to the n and p regions of the solar cell. Therefore, when the excess electrons from the n-region travel around the external circuit with the internal field E_0 and reach the p-region, they recombine with the excess holes on the p-side, generating electric current between the terminals.

The sunlight consists of a wide spectrum of wavelength of light, of which, the short wavelengths (visible light) generate the EHP at the n-region causing the excess holes to drift to the p-region through the depletion region. The spectrum of light with the ultraviolet wavelength gets absorbed to the depletion region and due to the drift occurring in that region, the EHP is separated allowing the excess holes to proceed towards the p-region and excess electrons

towards the n-region, inducing current. However, the long wavelengths consisting of the mid (3000 nm to 5000 nm) and far infrared wavelengths (between 8000 nm to 15000 nm) get absorbed directly to the p-region, and the EHP can only diffuse in the p-region as there is no built-in field to help in the drifting of charges [25].

These photon charges in the wide p-region move around and convert to cause damaging heat, reducing the life span of the solar cell and degrading the efficiency and performance of the solar cell [22]. However, adding an antireflection coating (ARC) of a thermally reflective material on the surface of the solar cell can help reflections of such unwanted wavelengths and transmit more light to the device.

ATO as an ARC is a highly conductive and transparent material for the visible range of light and also has low resistivity and TIR (Thermal Infrared Reflective) properties [38-45]. According to previous researchers, adding metal oxide sol-gels with ATO has the capability to increase infrared reflectivity and uniform coverage [46-48]. CoO-ATO has demonstrated favorable outcomes as a thin film ARC on carbon fibers [10]. It helps reflecting wavelengths of 3000-5000 nm and 8000-15000 nm from the surface. Based on the past outcomes, implications suggest that with the increase in the surface area, the infrared reflectivity increases [21].

Thin film solar cell technology is advancing due to its promising results of high efficiency. This research will help find optical and thermal characteristics of CoO-ATO to obtain better performance of photovoltaic cells. The results of each parameter will be compared amongst silicon substrates coated with CoO-ATO thin films and nanofiber membranes.

This work is inspired by a research drive to fabricate CoO-ATO thin film and nanofiber membranes to use for various applications such as solar cells, aircraft coatings and military purposes.

1.2 Hypothesis and Research Objectives

The following work demonstrates the preparation of CoO-ATO solutions with 8%, 10% and 12% by weight of ATO and variations between 0.2% to 2% by weight of cobalt oxide along with polystyrene and chloroform. These solutions are to be spin coated on silicon wafers and electro-spun. ATO being a transparent conductive material (TCO) shows property changes of the material when CoO is added.

Richard et. al. reported that the angular dependency of reflectance and hemispherical reflectance of CoO-ATO (where x% CoO is $0.2<x<0.5$) sol-gel coatings applied on carbon fiber mats are thermally reflective [10]. It is thereby *hypothesized* that CoO-ATO can probably act as an infrared shield for solar cells improving the overall efficiency and performance of ARCs, and as coatings, have minimum impact from thermal cycling.

In addition, scattered clouds and suspended particles in air result in a condition caused diffused light, which means that certain portions of light do not arrive at the surface of the solar cells in a straight line, but at an angle. This, in turn, means that all of the sun's illumination isn't reaching the solar cell to get converted to electricity and is lost [24]. By adding CoO-ATO nanofiber membranes, it can also be *hypothesized* that the diffused light will fall on the surface of the nanofibers at incident angles on the device and not be lost.

The *objectives* of this research are 1) to analyze the optical characteristics of CoO-ATO thin films and nanofiber membranes for different doping levels of CoO and ATO, 2) to perform UV-VIS (UV-Visible spectroscopy) and FTIR (Fourier Transform Infrared Spectroscopy) to complete a full spectrum characteristics of CoO-ATO and 3) to perform thermal cycling on all the doped thin films and re-test to find the possible impacts of temperature on the material.

1.3 Thesis Outline

The thesis comprises of eight chapters. Chapter one analyzes the background and motivation, research objectives and hypothesis. Chapter two identifies the selection of materials and properties. Chapter three elaborates on the preparation of the solution, the procedures for spin coating and electro-spinning the solution, the ideal parameters required to conduct the experiment and the results. Chapter four discusses the I-V measurements of a Si solar cell coated with a CoO-ATO thin film. Chapter five gives a brief introduction of the pre-thermal FTIR and UV-VIS characteristics, procedures to find respective parameters, the results, and a summary for each characteristic. Chapter six gives the FTIR and UV-VIS results post thermal cycling has been performed. Chapter seven gives parameters for electrospinning CoO-ATO nanofiber membranes as potential layers of a solar cell structure. Chapter eight is the final chapter including the overall thesis discussion, conclusion and future work.

2 CHOICE OF MATERIALS

Fabricating cobalt doped antimony doped tin oxide (CoO-ATO) thin films and nanofiber membranes are the main objective of this research. ATO mixed with cobalt oxide is in the form of a liquid, which can form thin films but not nanofibers. To produce nanofibers, we combine the liquid with a polymeric solution to be electrospun. Electrospinning is a process where a polymeric solution is electrically charged to form desired fibers. As the CoO-ATO solution has no polymer, it is mixed with polystyrene as a catalyst. A solvent is necessary to dissolve the polymer. There are many solvents for polystyrene like D-Limonene, toluene, acetone, chloroform, etc. Thereby, the various materials that can possibly be used for this application are discussed in this chapter.

2.1 Cobalt Oxide (CoO)

Figure 2: Cobalt oxide nano powder

Cobalt (II) oxide, CoO or cobalt monoxide is an inorganic compound and it is in the form of nano-powder whose particle size is 50 nm. It appears as a dark grayish or black in color. It is widely used in the ceramic industry to create enamels and glazes. It is also used in the chemical industry to produce cobalt salts. Cobalt oxide has a band gap of 2.4 eV. It is highly insoluble in water. Figure 2 shows the Cobalt oxide nano powder used for this research.

2.2 Antimony Doped Tin Oxide (ATO)

Antimony doped tin oxide ($SbSnO_2$) is thermally stable and highly insoluble. It can be available in different forms such as granulated, powder, tablet or liquid form. ATO, also a transparent conducting oxide (TCO) is known for its optical transmittance, wide energy band gap and high thermal conductivity. Due to the presence of these properties, these compounds can be highly used in solar cells and optical devices. In this research, the liquid form is used (Figure 3).

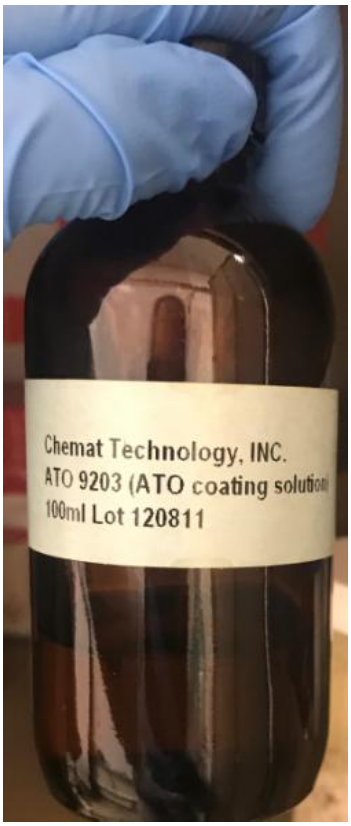

Figure 3: Antimony doped tin oxide

2.3 Polystyrene

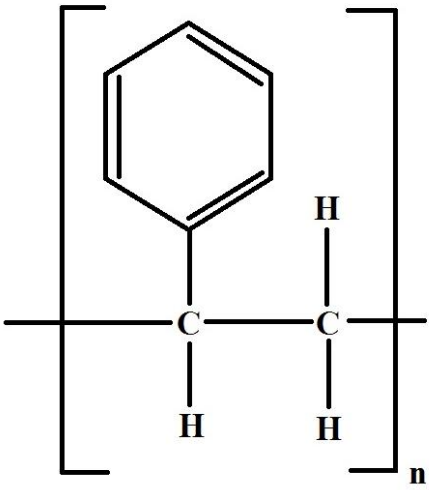

Figure 4: Structural representation of polystyrene

Polystyrene (PS) is a widely-used plastic in most industries and is a commonly found synthetic aromatic polymer. The form of PS used for this research is in the form of pellets. It can be available in forms of solids or foam. It obtains its form from styrene, which is a monomer. $(C_8H_8)_n$ is the chemical formula (Figure 4). Polystyrene has vivid applications, as it can be used as packaging material, appliances, electronics, medical, automotive, and many more.

2.4 Solvents

2.4.1 Chloroform

Chloroform or also known as trichloromethane, is a colorless, dense organic compound. $CHCl_3$ is its chemical formula (Figure 5). It is slightly soluble and non-flammable. It can be used as a solvent, reagent or in anesthetic procedures.

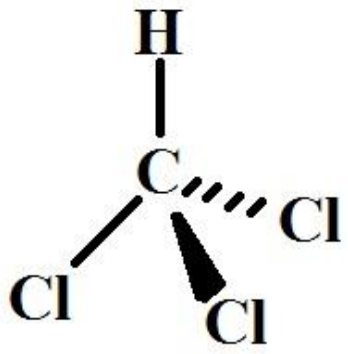

Figure 5: Structural representation of chloroform

2.4.2 D-Limonene (D-L)

D-limonene (D-L) is known to be an aromatic, colorless liquid hydrocarbon. Figure 6 shows the structural representation of D-limonene. This consists of a strong smell of oranges since it is formulated from citrus peels. The chemical formula is $C_{10}H_{16}$. It is insoluble in water and is a stable chemical.

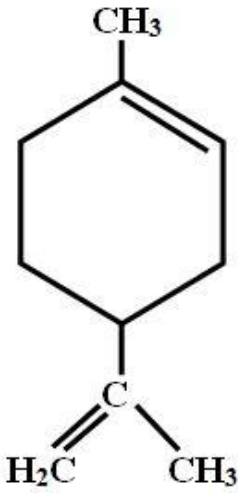

Figure 6: Structural representation of d-limonene

D-limonene has various uses. It can be used as an oral dietary supplement. It is recognized safe by the food and drug administration. It is also being used as a solvent to dissolve polystyrene.

2.4.3 Toluene

Toluene is another aromatic hydrocarbon which is colorless and is a water-insoluble liquid. It has a much-known smell similar to paint thinners. It is also known as methylbenzene. Figure 7 shows the structure of toluene. Its chemical formula is C_7H_8. It is widely used as a solvent.

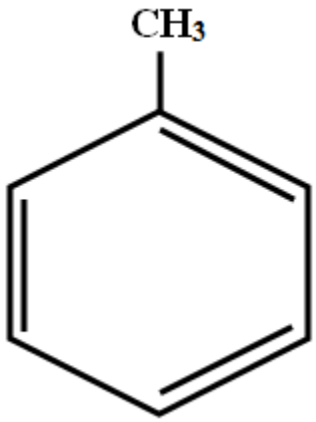

Figure 7: Structural representation of toluene

2.5 Summary

After a literature review on all the properties of all the possible solvents, chloroform was finalized to be used along with polystyrene, as the polymer, for this research, due to its ability to dissolve PS into a homogenous solution and promote the electrospinning of PS, as compared to D-limonene and toluene. Therefore, this entire research is based on findings of electrical, optical and thermal characteristics of CoO-ATO along with PS dissolved in $CHCl_3$.

3 SPIN COATING PROCESS

3.1 Composition of the Solution

Based on the favorable results received from Richard [10] and Devisetty [21] in using a CoO-ATO solution of different weight % of CoO ranging from 0.2% to 2% to demonstrate anti-reflectivity in IR range and fabrication of nanofibers, respectively. Three batches of solutions were prepared to make thin films and nanofibers. Each batch consisted of 8 different weight % of CoO ranging from 0.2% to 2%. The three batches differed with the ATO weight %, thereby, having the first batch with 8% by weight ATO, second batch with 10% by weight ATO and third batch with 12% by weight ATO.

The procedures to make all the solutions were the same except that the weights of all the compounds were to be calculated accurately to 0.0001 of a gram (table 1, 2 and 3).

The CoO nano-powder and PS in the form of pellets are measured using the weighing scale and are put in glass vials. ATO is weighed and added using a syringe. Then using a 27-gauge needle, chloroform is added to the same solution and tightly sealed in the vial. A 6 mm x 25 mm magnetic stirrer is dropped into each of the vials.

To prevent evaporation, closing the lids tightly is a must. The bottles are then kept on a magnetic stirrer. PS dissolves very quick as chloroform is a good solvent of polystyrene.

To obtain the high level of homogeneity of the solution, it is stirred for almost 6-8 hours or until CoO is completely mixed into the solution. Figure 8 below shows the solutions on the magnetic stirrer/hot plate.

Table 1: Measurements for solutions of 8% weight ATO

PS (%wt)	ATO (%wt)	CoO (%wt)	CHCl3 (%wt)
13.77	8	0.2	78.03
13.725	8	0.5	77.775
13.695	8	0.7	77.605
13.65	8	1	77.35
13.605	8	1.3	77.095
13.575	8	1.5	76.925
13.53	8	1.8	76.67
13.5	8	2	76.5

Table 2: Measurements for solutions of 10% weight ATO

PS (%wt)	ATO (%wt)	CoO (%wt)	CHCl3 (%wt)
13.47	10	0.2	76.33
13.425	10	0.5	76.075
13.395	10	0.7	75.905
13.35	10	1	75.65
13.305	10	1.3	75.395
13.275	10	1.5	75.225
13.23	10	1.8	74.97
13.2	10	2	74.8

Table 3: Measurements for solutions of 12% weight ATO

PS (%wt)	ATO (%wt)	CoO (%wt)	CHCl3 (%wt)
13.17	12	0.2	74.63
13.125	12	0.5	74.375
13.095	12	0.7	74.205
13.05	12	1	73.95
13.005	12	1.3	73.695
12.975	12	1.5	73.525
12.93	12	1.8	73.27
12.9	12	2	73.1

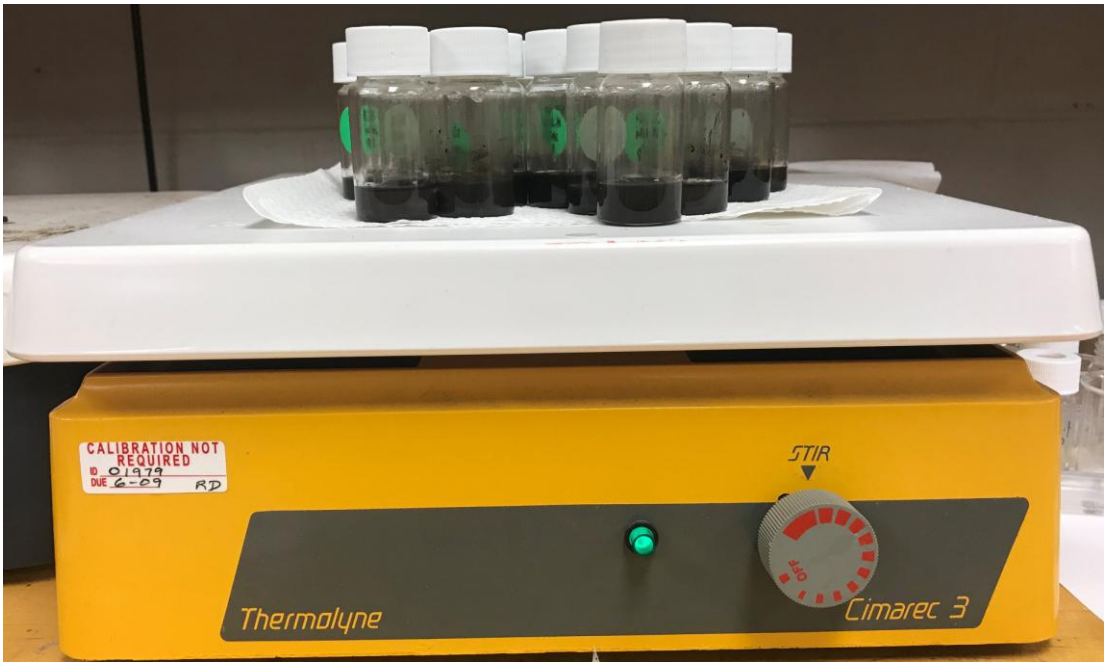

Figure 8: Solutions on the magnetic stirrer

3.2 Procedure

For the spin coating process, we utilize the spin coater model P6700. With the help of this spin coater, we set a recipe of the ideal speed (in rpm) and time (in seconds) that is required to spin the substrates and obtain a desirable uniform coating on the entire silicon wafer.

The spin coater is connected to a vacuum to let the substrate sit on the chuck and not fly amidst the process. The spin coating machine is covered with aluminum foil to avoid chemical deposition on the sides of the spin coater. The sample/silicon substrate is placed on the chuck and the solutions are poured on the substrate to cover the entire area. Then the spin coater lid is closed and the machine is turned on. Once the spin coating process is completed, the substrates are allowed to cool down and checked for uniformity. Figure 9 shows the spin coating machine.

Figure 9: Spin coater P6700

3.3 Ideal Parameters

The spin coating parameters we use in the spin coater is as follows: The ramp up process starts by reaching a speed of 1000 rpm in 5 seconds and increases to 4000 rpm in the next 5 seconds. For the next 60 seconds, the solution is allowed to spin on the silicon substrate at a speed of 4000 rpm to obtain uniform coating. The last 10 seconds is to slow down the speed and reduce it eventually to zero. Figure 10 shows the recipe in the form of a step-up graph where Ramp 1 is when the speed reaches 1000 rpm in 5 seconds (T1); Ramp 2 is when the speed reaches 4000 rpm in the next 5 seconds (T2); Ramp 3 is when the speed is constant at 4000 rpm for the next 60 seconds (T3) and then in the next 10 seconds (T4) the speed is reduced to 0.

RECIPE	00001
RPM1	01000
RAMP1	00005
TIME1	00000
RPM2	04000
RAMP2	00005
TIME2	00004
RPM3	04000
RAMP3	00005
TIME3	00056
TIME4	00010
SOLVENT	00000
N2	00000
COATING	00000

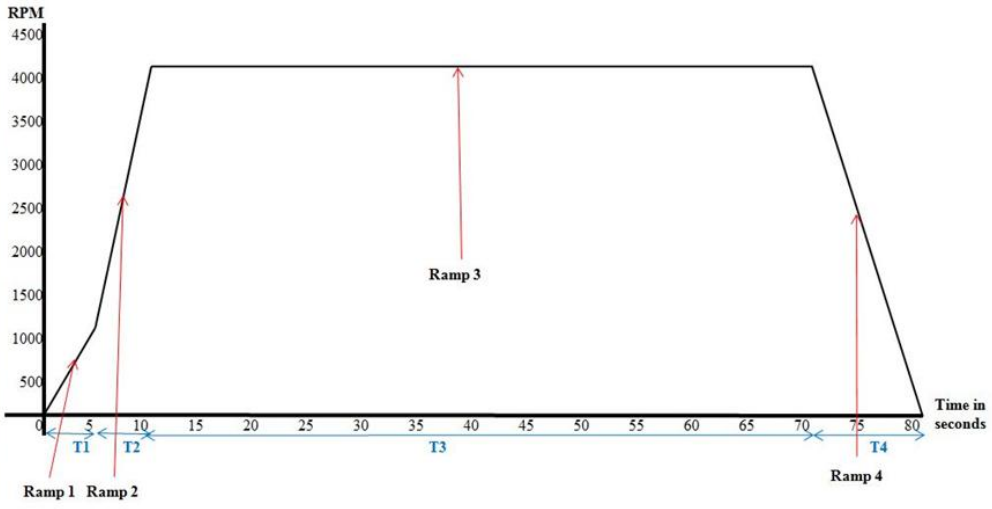

Figure 10: Recipe cycle used to spin coat

3.4 Results

Spin coating was performed on 1 x 1 inch n-type <100> silicon wafers with solutions of 8%, 10% and 12% by weight ratio of ATO, and figure 11 shows the uniform coating of all solutions on the silicon substrates. The average thickness that was observed through SEM technique of the spin coated samples was 495 nm for 10% ATO. These spin coating parameters will be used for conducting the optical characteristics and coating solar cells.

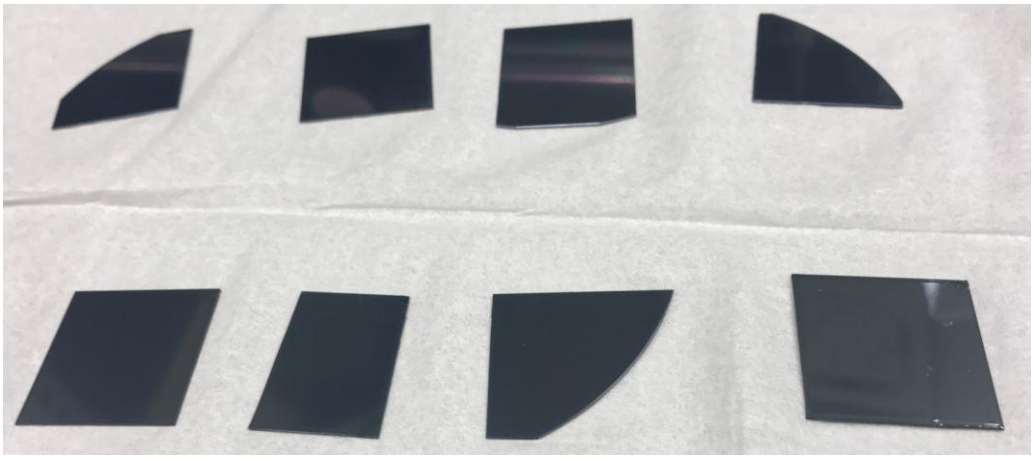

Figure 11: Spin coated silicon wafers

4 ELECTRICAL CHARACTERIZATION OF CoO-ATO STRUCTURES

4.1 Introduction

From this chapter, preliminary electrical properties will be investigated for high efficiency and promising features for solar cell technology. Thin film devices are well known to be resolving alternative energy problems. In this chapter, the electrical characteristics, i.e. I_{SC} (short circuit current) versus V_{OC} (open circuit voltage) will be observed.

The PV cell, when open circuited, means that it is not affixed to any external load, the current is at its minimum value (zero) and the maximum voltage across the cell obtained is the open circuit voltage, V_{OC}. Similarly, the voltage is made minimum (zero) when the PV cells are short circuited by connecting both the leads (negative and positive) together and the maximum current measured across the PV cell is known as the short circuit current, I_{SC} [26].

4.2 I-V Characteristics

To measure the I_{SC} vs. V_{OC}, the solar cells were coated with CoO-ATO thin films of average thickness of 495 nm and nanofibers and the contacts were connected to copper tape. All the coated solar cells were kept in bright sunlight and the voltages and currents were measured using a multimeter. This was done until the readings were stabilized, for approximately 1 minute each.

ATO, as mentioned earlier is a transparent conducting oxide (TCO) and is thermally stable up to 400 degrees Celsius and can also reflect the infrared spectrum that if absorbed by the solar cell, can cause damaging heat. ATO is relatively of a lesser cost when compared to Indium

doped Tin Oxide (ITO) and Fluorine doped Tin Oxide (FTO). When CoO is added to ATO, the combination of both makes it easier to reflect the infrared rays of light, allowing maximum absorption as observed in table 4. It is evident that the maximum wattage power is produced by the 16% CoO mixed with 84% ATO [14].

Table 4: Power generated by photovoltaic cells [14]

CoO + ATO (wt %)	**V_{OC} (V)**	**I_{SC} (A)**	**Power (W)**
4% CoO + 96% ATO	0.558	1.077	0.600
8% CoO + 92% ATO	0.556	1.084	0.602
12% CoO + 88% ATO	0.520	1.200	0.624
16% CoO + 84% ATO	0.537	1.460	0.784

These electrical results further demonstrate the ability of CoO-ATO to enhance the performance of solar cells. For future works, a TCO nanofiber membrane can be investigated on their performances.

5 OPTICAL CHARACTERIZATION OF CoO-ATO STRUCTURES

5.1 Introduction

From this chapter, we will utilize FTIR (Fourier Transform Infrared Spectroscopy) and UV-VIS spectroscopy to determine the first known optical properties of CoO-ATO, inclusive of the energy band gap of the material.

The technique used to measure the amount of light being transmitted or absorbed by any sample at particular wavelengths is known as FTIR spectroscopy. This technique provides the unknown components in the solution, the quality of each component and the component amount.

UV-VIS spectroscopy is the technique used to determine the absorption properties and energy band gap of the material in the range of ultraviolet and visible light spectrum wavelength. The combination of these characterization techniques will provide a view over the entire spectrum (300 – 15000 nm).

5.2 FTIR

To perform FTIR spectroscopy, the solutions are spun coated on the silicon substrates and dried up. The FTIR spectroscopy used for this experiment is the Perkin Elmer Spectrum One FTIR spectrometer. The spectrometer is switched on and with the help of the software, the baseline measurements are performed for the mirror setup. The samples are then placed in the spectrometer and the scan is performed. This is repeated for all the samples and the results are stored and analyzed. According to previous researchers, FTIR has been performed separately on ATO and CoO respectively.

Tin oxide has been doped with different % by weight of Antimony and FTIR has been performed. The peaks consisting of wave numbers 400-800 cm^{-1} are the characteristic peaks of the presence of ATO particles. With an increase in antimony doping in the tin oxide, the single peaks that occur will change to double peaks. Table 5 shows the FTIR absorption peaks for ATO with different levels of doping of Antimony. The various peaks at various wave numbers show the functional groups present in the compound. The peaks at 1400 cm^{-1} show that N-H bend due to the presence of Ammonium Hydroxide. Similarly, the presence of Antimony can be seen at 600 cm^{-1} and tin oxide particles peak can be seen at wave numbers between 600 cm^{-1} and 750 cm^{-1}. At 0% Sb doping, we can see that it is a single peak and with the increase in Sb doping, it forms double peaks for the presence of ATO particles [27].

Table 5: FTIR spectrum for different doping levels of Sn in ATO [27]

Wavenumbers (in cm-1)	Functional groups
3500	O-H Stretch
1400	N-H bend
750-600	Tin oxide particles
600	Antimony particles
400-800	ATO particles

CoO has an impact on the absorbance as well. The sharp peaks found close to 580 cm^{-1} show the presence of Cobalt oxide in ATO [35]. Table 6 shows the FTIR spectrum for CoO. The peaks that were observed between 863 cm^{-1} to 430 cm^{-1} represented the vibrations of metal oxide. At 3426 cm^{-1}, the peaks represent hydrogen-bonded hydroxyl groups. Another peak at 1634 cm^{-1} is due to the bending of water molecules [33].

Table 6: FTIR spectrum for CoO [33]

Wavenumbers (in cm-1)	Functional groups
3426	O-H Stretch
1634	Bend due to water molecules
863-430	Vibrations of metal oxide

From the previous works of individual FTIR spectrums of ATO and CoO, the presence of CoO-ATO should be mainly between the approximate wave numbers of 850 cm^{-1} to 430 cm^{-1}. In accordance with the Beer's law, absorbance is the logarithmic value of transmission inverse, i.e. A=log (1/T). Absorbance is also linearly proportional to the concentration of material. Figure 12, 13 and 14 represent the pre-thermal absorbance results for 8%, 10% and 12% ATO respectively along with the lowest (0.2%) and highest (1.8%) concentration of CoO.

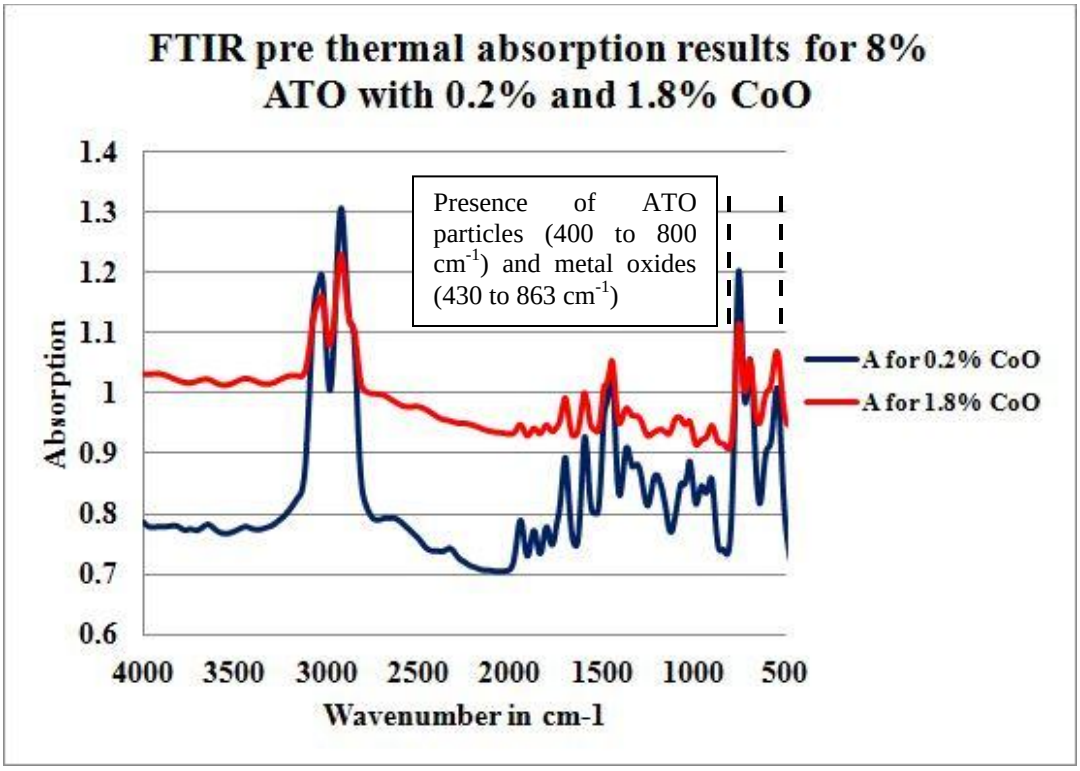

Figure 12: Pre-thermal FTIR absorption results for 8% ATO with 0.2% and 1.8% CoO

From figure 12, data obtained shows that the absorbance at a wavelength of 2500 nm (4000 cm^{-1}) for 8% ATO with 0.2% CoO results in 78% absorbance and 103% absorbance with 1.8% CoO. The IR wavelength targeted is above 8000 nm (1200 cm^{-1}). Therefore, the amount of light absorbed at 1200 cm^{-1} is 81% for 0.2% CoO and 93% for 1.8% CoO. From figure 13, at 4000 cm^{-1} absorbance for 10% ATO with 0.2% CoO is around 74% and 85% absorbance is for 10% ATO and 1.8% CoO. At 1200 cm^{-1}, 65% absorbance is observed for 0.2% CoO and 85% is observed for 1.8% CoO.

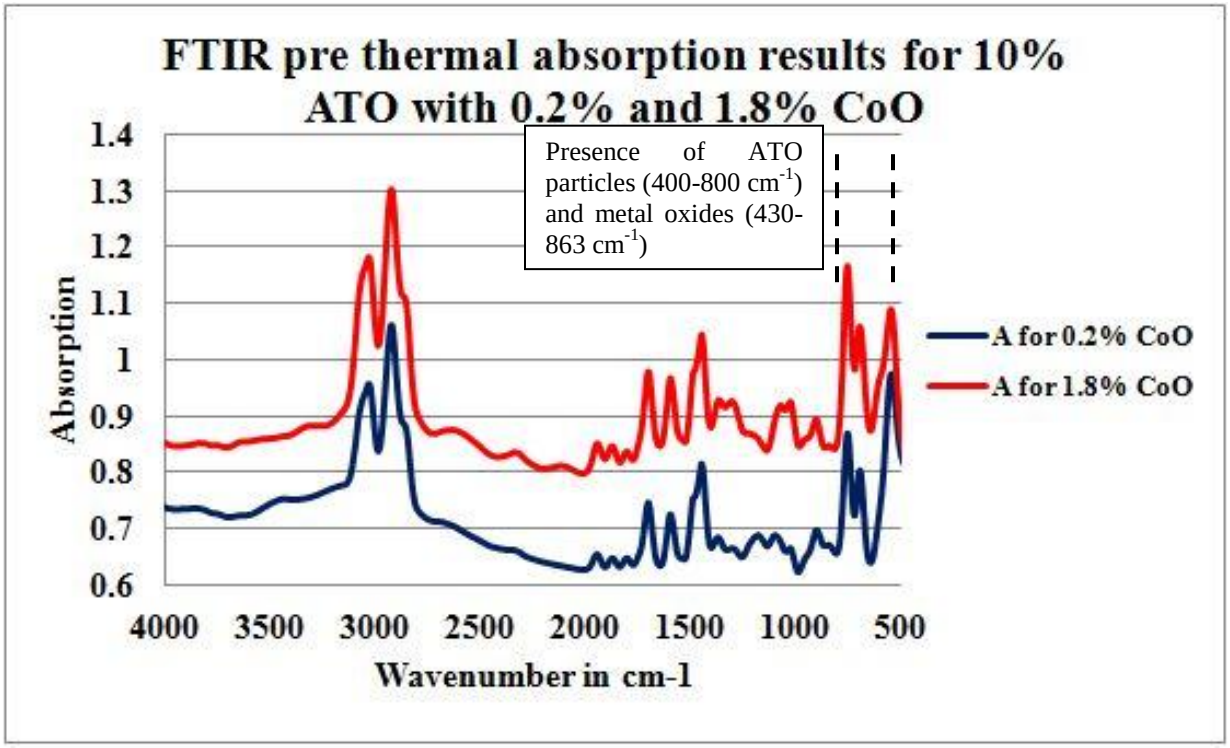

Figure 13: Pre-thermal FTIR absorption results for 10% ATO with 0.2% and 1.8% CoO

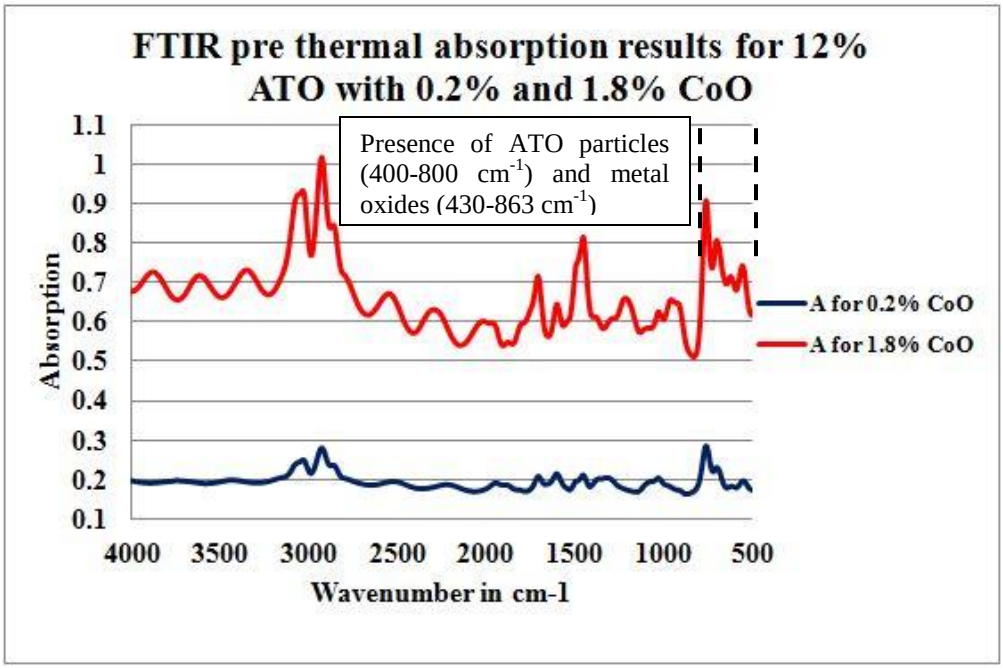

Figure 14: Pre-thermal FTIR absorption results for 12% ATO with 0.2% and 1.8% CoO

From figure 14, it can be concluded that 20% absorbance occurs with 12% ATO and 0.2% CoO whereas 68% absorbance occurs for 12% ATO with 1.8% CoO. At 1200 cm^{-1}, 18% light is absorbed for 0.2% CoO and 58% light is absorbed for 1.8% CoO.

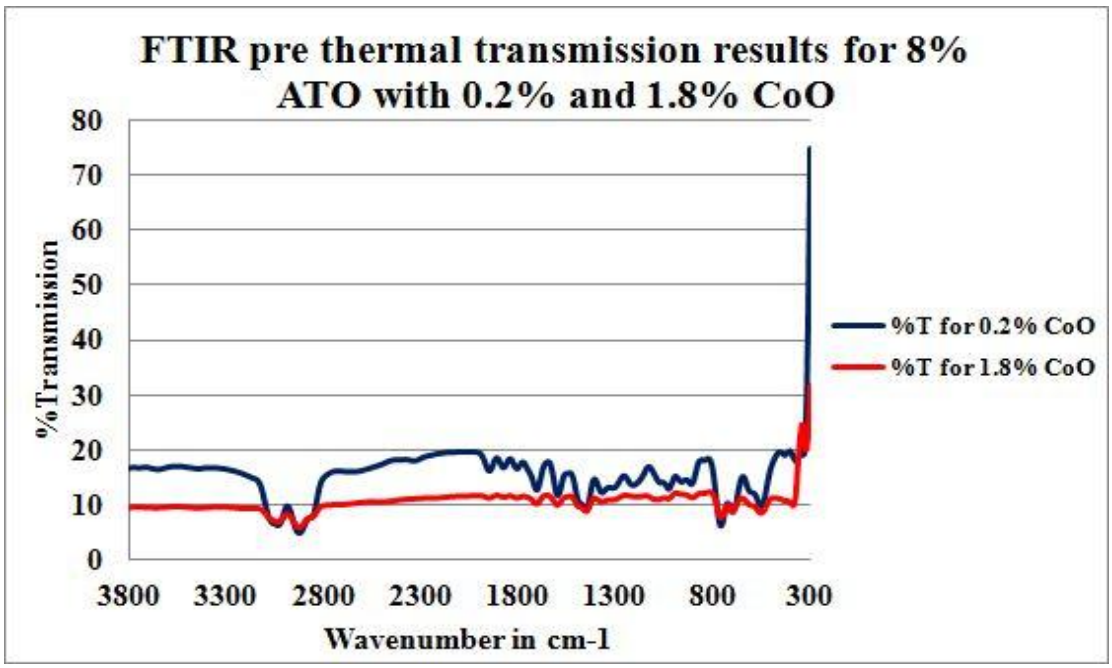

Figure 15: Pre-thermal FTIR transmission results for 8% ATO with 0.2% and 1.8% CoO

Transmission is defined as the amount of light that passes through a material or substance. Figures 15, 16 and 17 show the pre-thermal transmission results. As per figure 15, at 4000 cm^{-1} and 1200 cm^{-1}, 16% and 10% IR light transmits for 8% ATO with 0.2% CoO and 1.8% CoO respectively. In figure 16, at 4000 cm^{-1} and 1200 cm^{-1}, 18% and 15% light transmits for 10% ATO with 0.2% CoO and 1.8% CoO respectively. Similarly, in figure 17, at 4000 cm^{-1} and 1200 cm^{-1}, 64% and 20% light transmits for 12% ATO with 0.2% CoO and 1.8% CoO respectively.

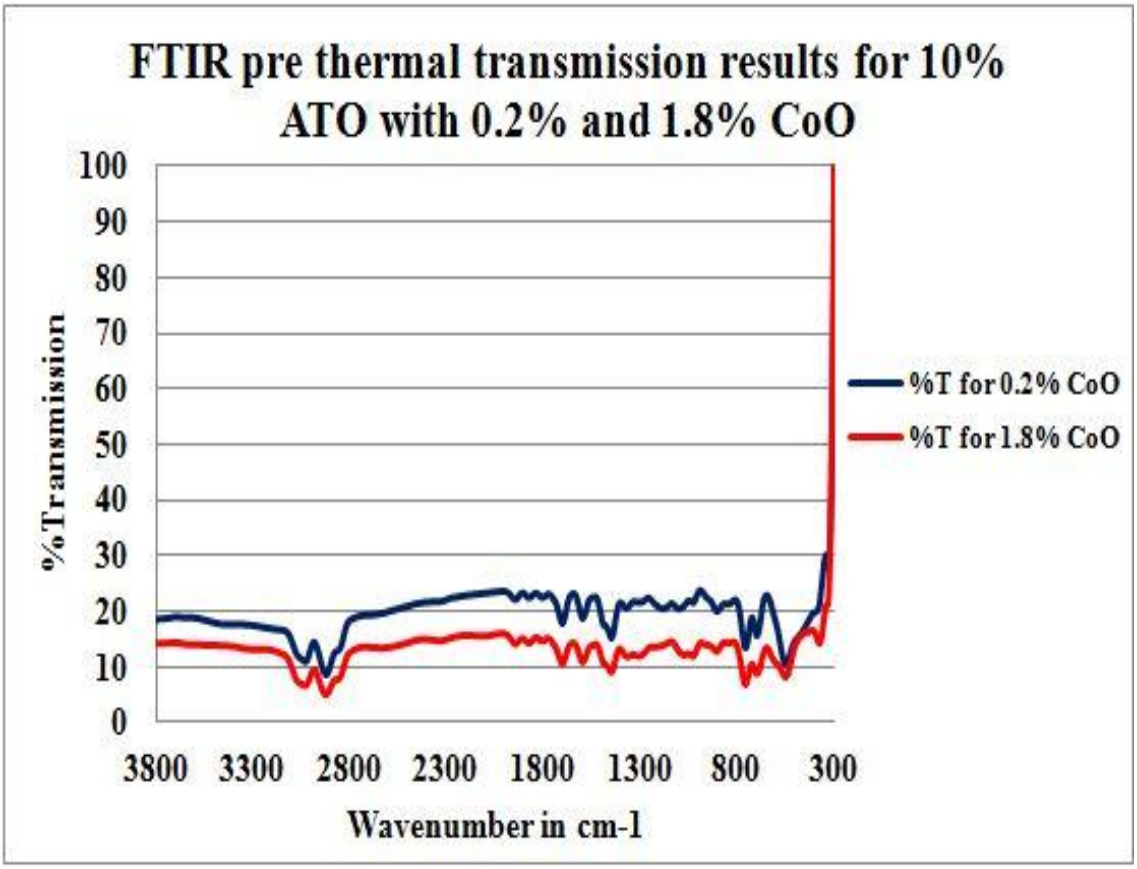

Figure 16: Pre-thermal FTIR transmission results for 10% ATO with 0.2% and 1.8% CoO

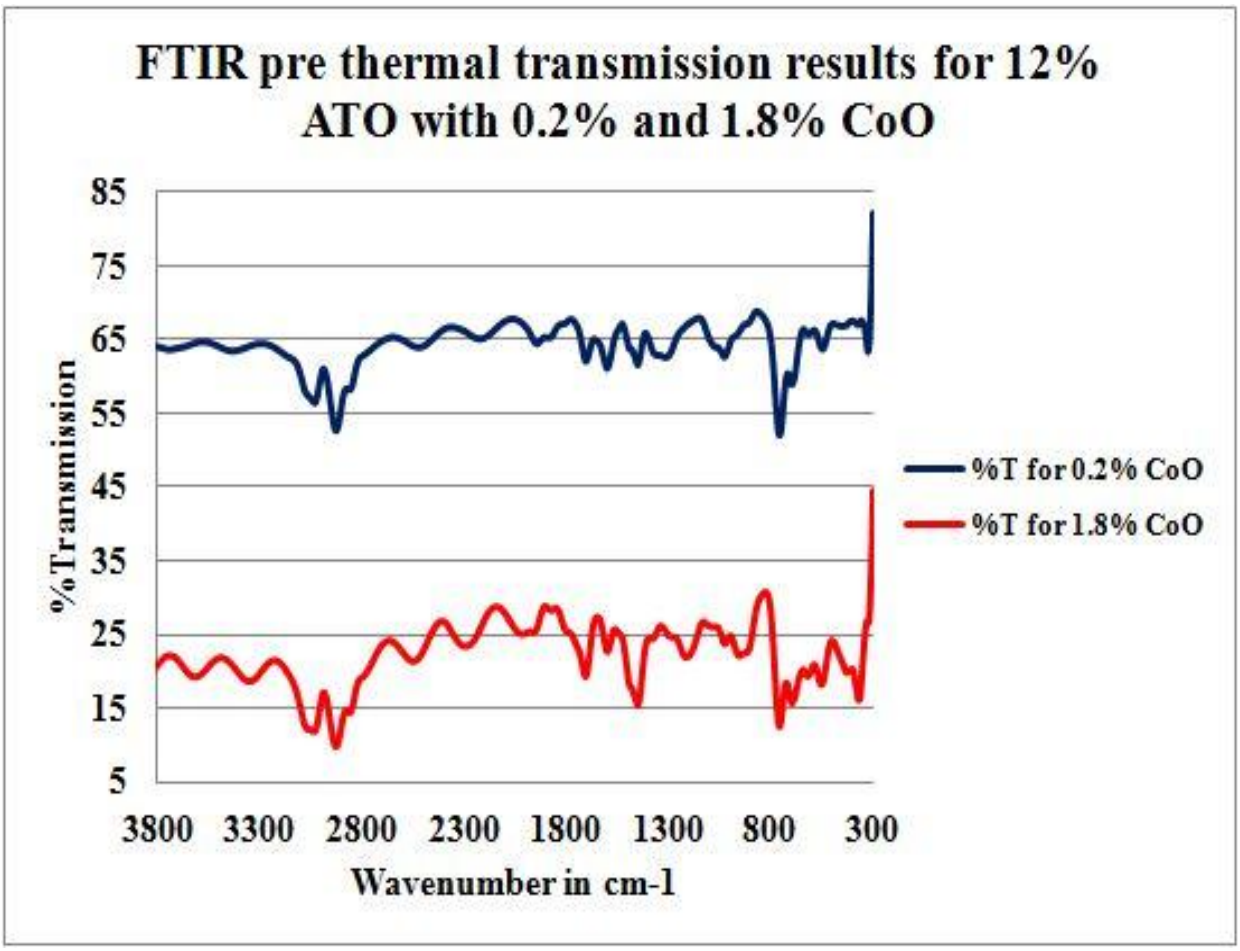

Figure 17: Pre-thermal FTIR transmission results for 12% ATO with 0.2% and 1.8% CoO

5.3 UV-VIS

The UV-VIS spectrometer used is the Jasco V-530 spectrometer. The solutions are coated on glass slides to perform this set of measurements. The baseline and absolute measurements are performed after switching on the system. The glass slides are then placed in the spectrometer and a laser of light passes over the material to observe the results.

The energy band gap of a material can be determined from the UV-VIS graphs. The band gap calculated for ATO was found to be about 4.62 eV at an absorption wavelength of 260 nm [36]. Similarly, the band gaps of CoO were found to be 1.58 and 3.79 eV [37]. Table 7 summarizes the UV-VIS results for CoO and ATO.

Table 7: UV-VIS results for ATO and CoO [36-37]

Material	Absorption Wavelength	Band gap
ATO	260 nm	4.62 eV
CoO	783-327 nm	1.58-3.79 eV

The band gap is calculated with the formula, $E = (hc)/\lambda$ where h=Planck's constant of 6.624×10^{-34} m^2 kg/s, c=speed of light (3×10^8 m/s) and λ is the absorption wavelength.

Figures 18, 19 and 20 give the pre-thermal UV-VIS results of 8%, 10% and 12% ATO with 0.2% and 1.8% CoO respectively. In figure 18, the absorption wavelength is 380 nm, for which the band gap estimated is 3.26 eV. For figure 19, the absorption wavelength is 400 nm which gives a band gap of 3.10 eV. For 12% ATO, in figure 20, the absorption wavelength is 410 nm that calculates a band gap of 3.02 eV.

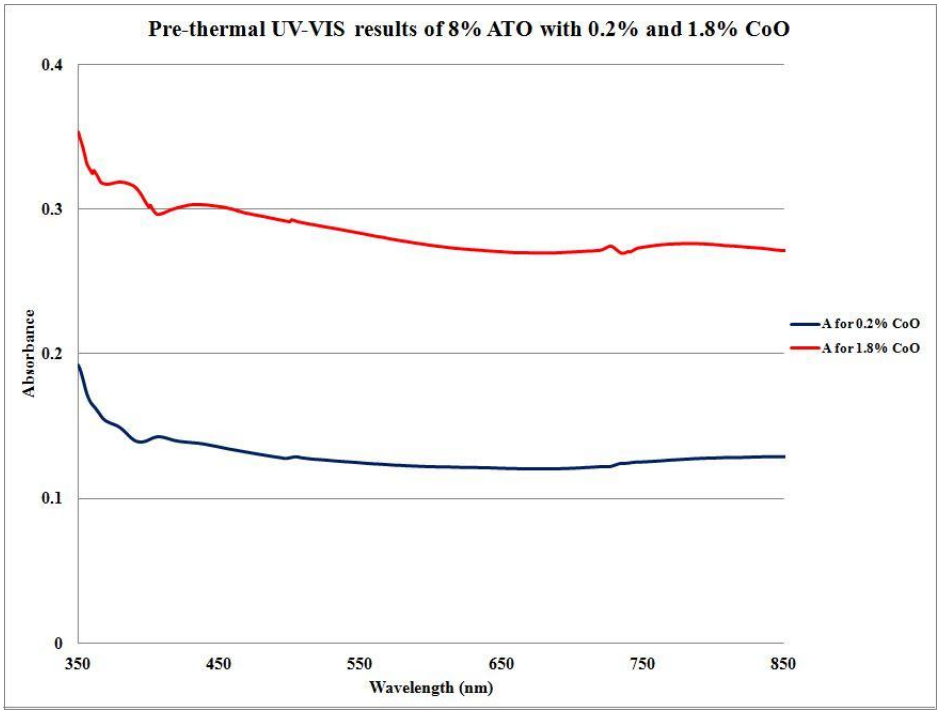

Figure 18: Pre-thermal UV-VIS absorption results for 8% ATO with 0.2% and 1.8% CoO

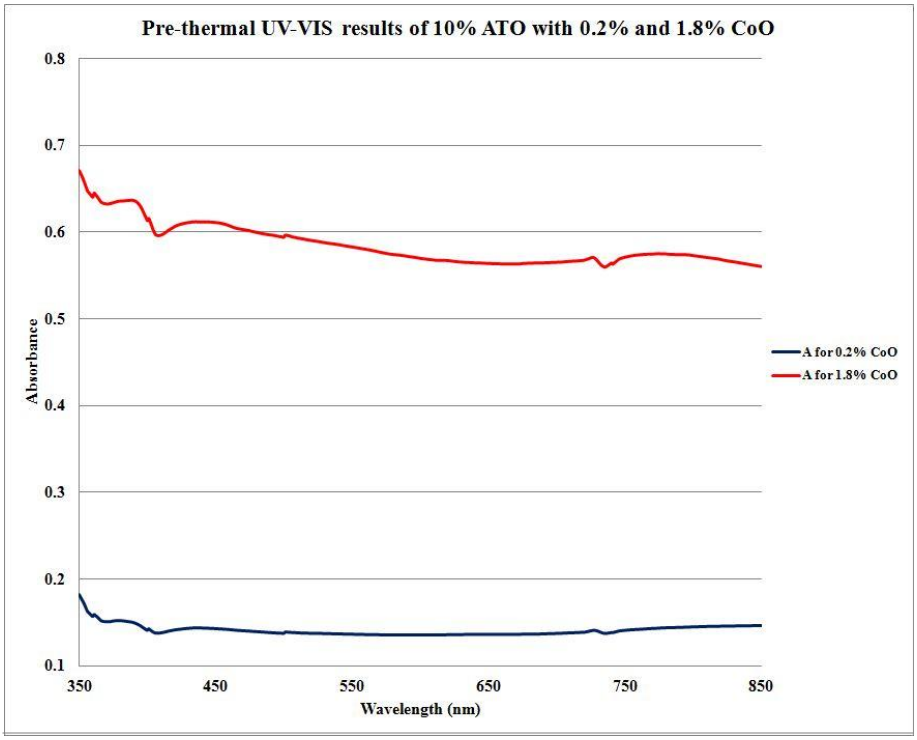

Figure 19: Pre-thermal UV-VIS absorption results for 10% ATO with 0.2% and 1.8% CoO

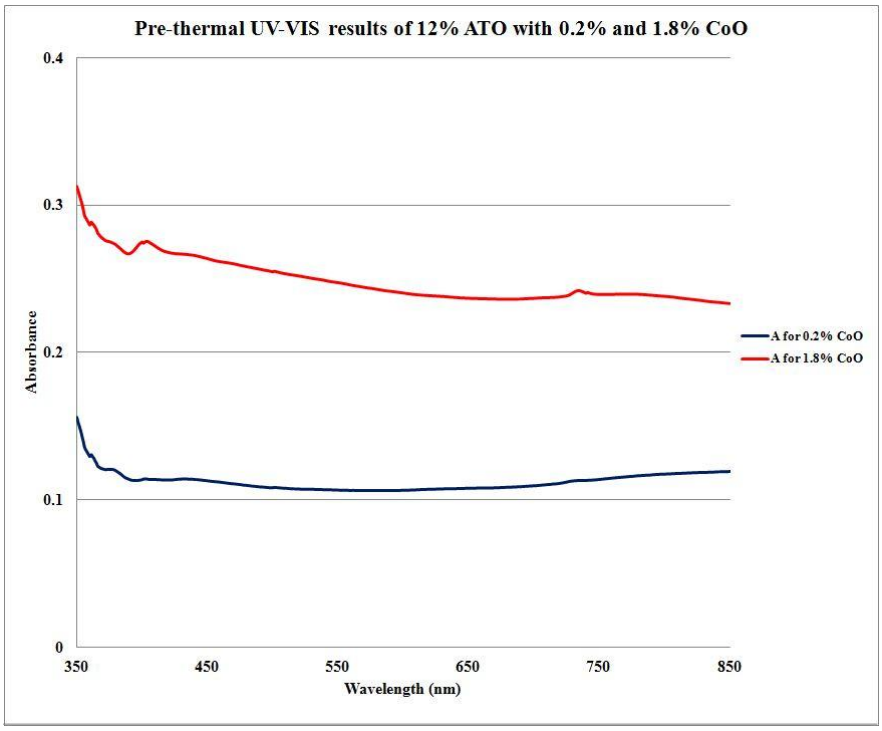

Figure 20: Pre-thermal UV-VIS absorption results for 12% ATO with 0.2% and 1.8% CoO

5.4 Summary

By conducting FTIR and UV-Vis measurements, the optical properties of CoO-ATO for thin films can be easily studied.

From FTIR, it can be summarized that the solution with 8% ATO and 1.8% CoO has the highest absorbance and lowest transmittance. The solution with 12% ATO and 0.2% CoO has the lowest absorbance and highest transmittance. Also comparing the individual FTIR spectrums of ATO and CoO, and the FTIR spectrum of CoO-ATO, we can conclude that the bends of different functional groups has a match of presence of both ATO and CoO compounds.

The UV-VIS data infers that the energy band gap reduces with an increase in the concentration of ATO. The solutions with 8%, 10% and 12% ATO had 380 nm, 400 nm and 410 nm as the absorption wavelength respectively which calculated a band gap of 3.2 eV, 3.10 eV and 3.02 eV respectively.

6 THERMAL CYCLING IMPACT ON CHARACTERISTICS OF CoO-ATO

6.1 Introduction

The photovoltaic industry's concerns are growing with the popularity of solar cell technology. The pressure builds even more with the high demands of developing the portability, high-integrity, life span and efficiency. However, they are also encountering another challenge. The solar cells are potentially unable to withstand higher temperatures. Due to this, it is primarily important to perform thermal cycling to test any thin film coating that is being added to the manufacturing of solar cells. Testing the materials of withstanding high temperatures of 85 degree Celsius helps understand the nature of the material to be applied to the photovoltaic cells. Thermal cycling is studied to understand if photovoltaic cells can withstand different climates.

In this chapter, the solar cells, glass slides and silicon wafer samples coated with CoO-ATO has been thermally tested at a temperature of 85 degree Celsius and retested for results of FTIR and UV-VIS spectroscopy. The results are compared and tested for advantages and disadvantages in this chapter.

6.2 FTIR

The samples as mentioned were treated at 85 degrees Celsius and tested for FTIR and UV-VIS to validate the performance of the material under thermal treatment.

From figure 21, data obtained shows that the absorbance at a wavelength of 2500 nm (4000 cm^{-1}) for 8% ATO with 0.2% CoO results in 12% absorbance and 60% absorbance with 1.8% CoO. The amount of light absorbed at 1200 cm^{-1} is 12% for 0.2% CoO and 1.8% CoO.

From figure 22, at 4000 cm^{-1} absorbance for 10% ATO with 0.2% CoO is around 27% and 47% absorbance is for 10% ATO and 1.8% CoO. At 1200 cm^{-1}, 25% absorbance is observed for 0.2% CoO and 1.8% CoO.

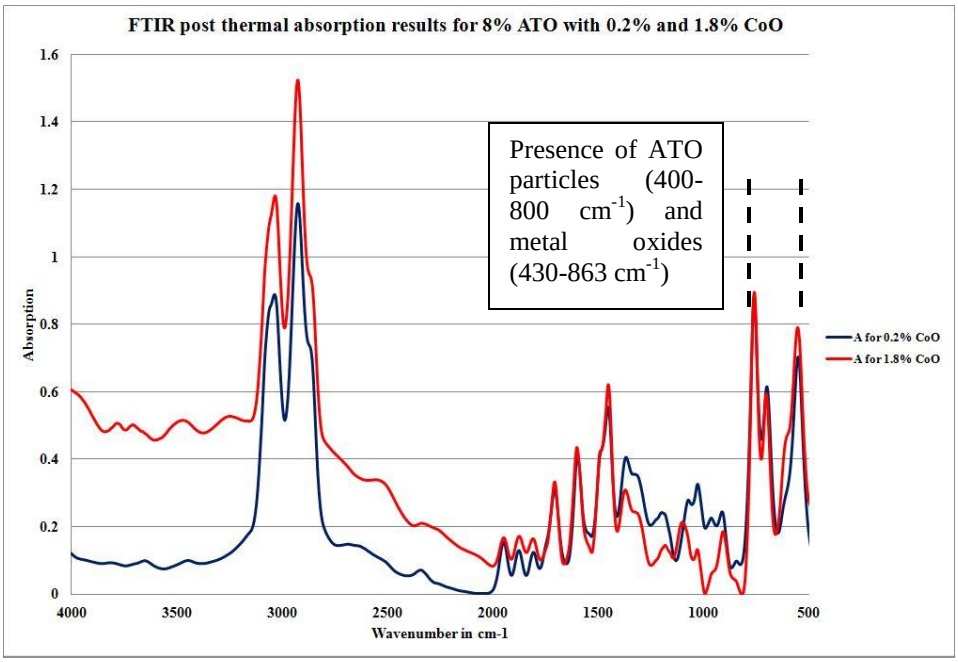

Figure 21: Post thermal FTIR absorption results for 8% ATO with 0.2% and 1.8% CoO

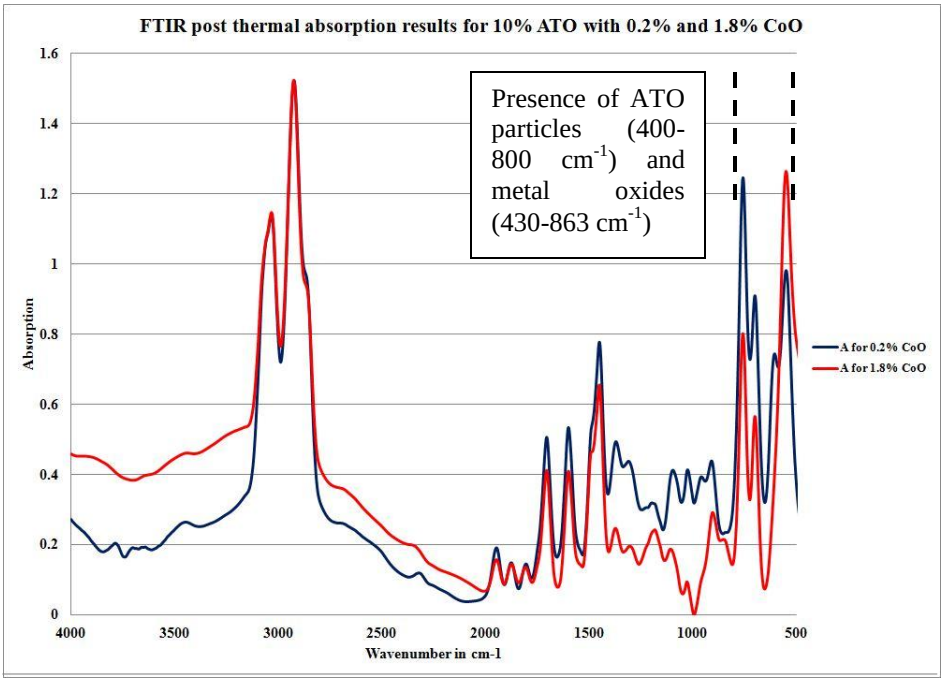

Figure 22: Post thermal FTIR absorption results for 10% ATO with 0.2% and 1.8% CoO

From figure 23, it can be concluded that at 4000 cm^{-1} 35% absorbance occurs with 12% ATO and 0.2% CoO whereas 67% absorbance occurs for 12% ATO with 1.8% CoO. At 1200 cm^{-1}, 10% light is absorbed for 0.2% CoO and 1.8% CoO.

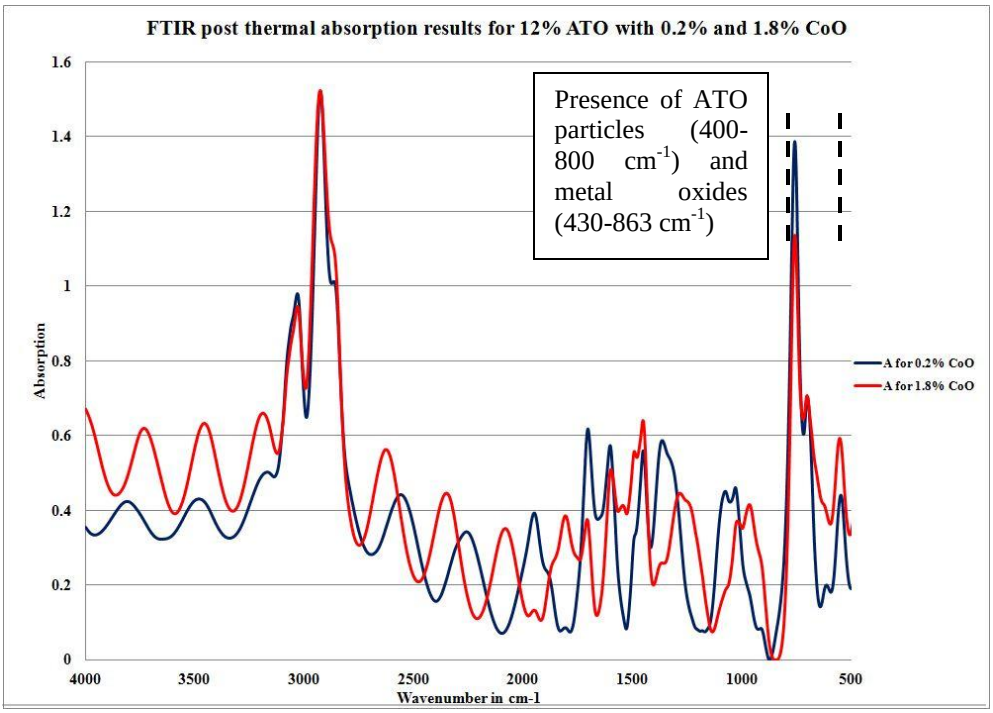

Figure 23: Post thermal FTIR absorption results for 12% ATO with 0.2% and 1.8% CoO

Figures 24, 25 and 26 show the post-thermal transmission results. As per figure 24, for 8% ATO with 0.2% CoO and 1.8% CoO with wave numbers at 4000 cm^{-1} and 1200 cm^{-1}, 32% and 82%, 58% and 72% IR light transmits respectively. In figure 25, for 10% ATO with 0.2% CoO and 1.8% CoO with wave numbers at 4000 cm^{-1} and 1200 cm^{-1}, 64% and 38%, 50% and 70% IR light transmits respectively. Similarly, in figure 26, for 12% ATO with 0.2% CoO and 1.8% CoO with wave numbers at 4000 cm^{-1} and 1200 cm^{-1}, 38% and 32%, 35% and 45% IR light transmits respectively.

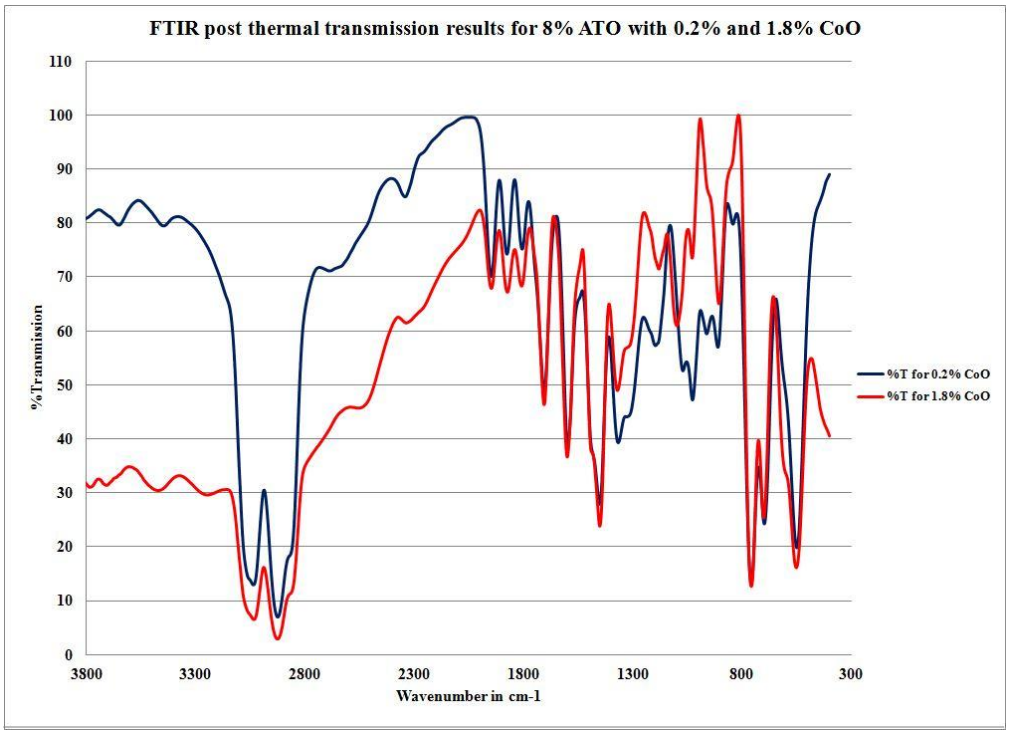

Figure 24: Post thermal FTIR transmission results for 8% ATO with 0.2% and 1.8% CoO

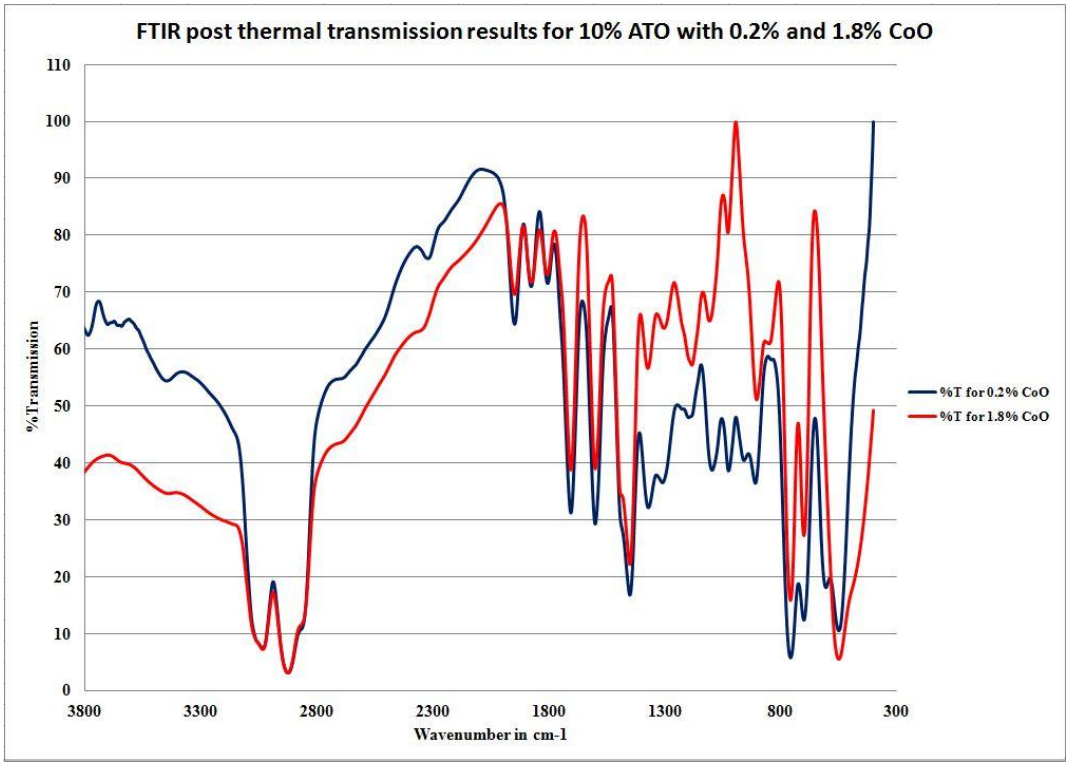

Figure 25: Post thermal FTIR transmission results for 10% ATO with 0.2% and 1.8% CoO

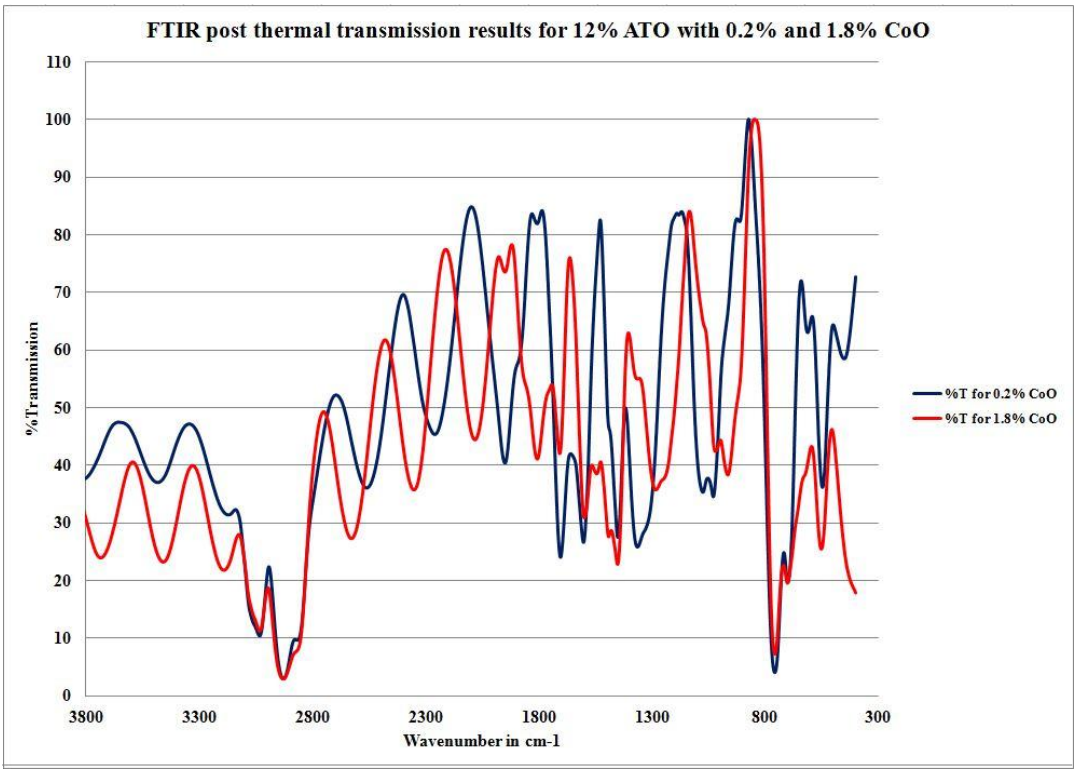

Figure 26: Post thermal FTIR transmission results for 12% ATO with 0.2% and 1.8% CoO

6.3 UV-VIS

Figures 27, 28 and 29 give the pre-thermal UV-VIS results of 8%, 10% and 12% ATO with 0.2% and 1.8% CoO respectively. In figure 27, the absorption wavelength is 500 nm, for which the band gap estimated is 2.48 eV. For figure 28, the absorption wavelength is 490 nm which gives a band gap of 2.53 eV. For 12% ATO, in figure 29, the absorption wavelength is 480 nm that calculates a band gap of 2.58 eV.

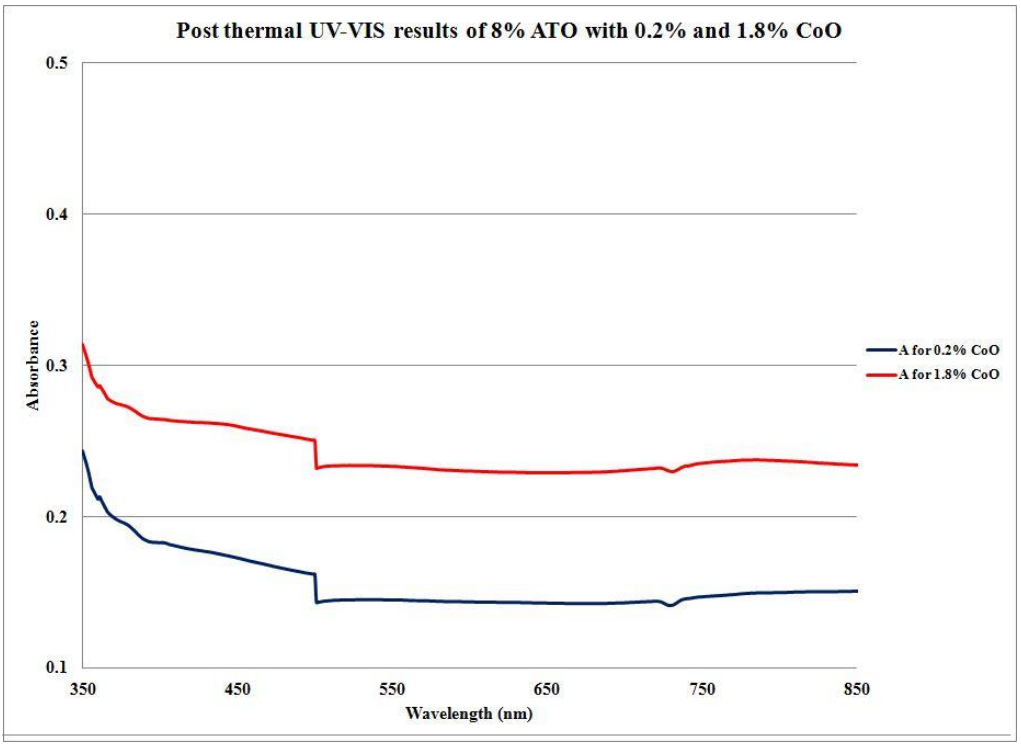

Figure 27: Post thermal UV-VIS absorption results for 8% ATO with 0.2% and 1.8% CoO

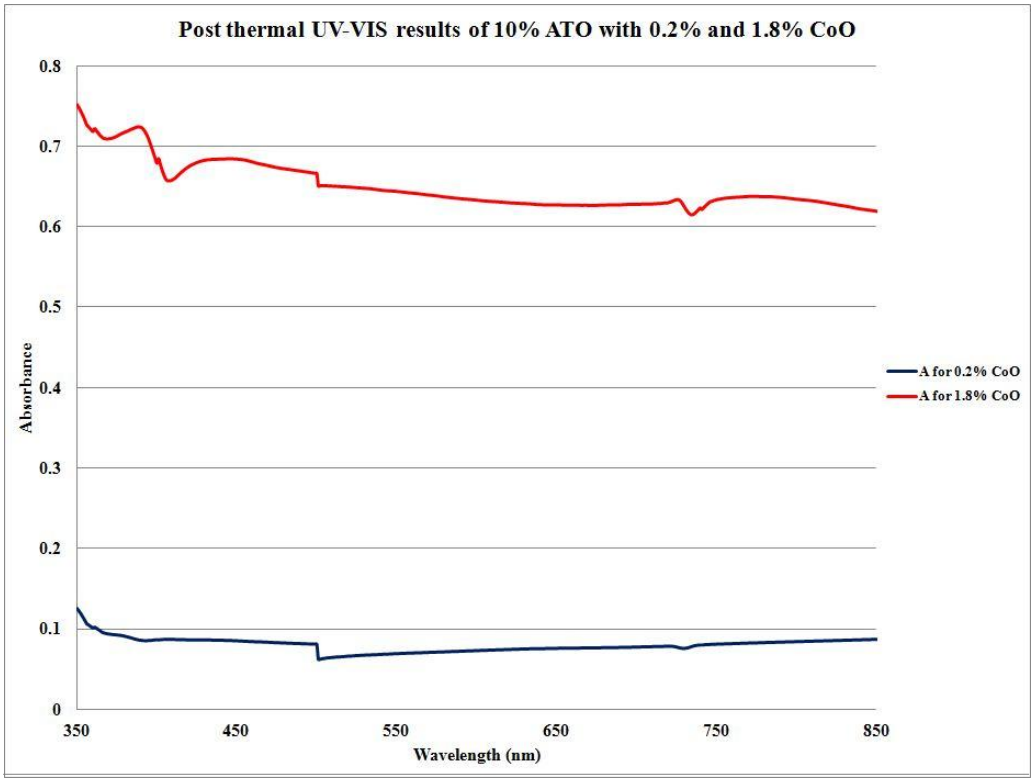

Figure 28: Post thermal UV-VIS absorption results for 10% ATO with 0.2% and 1.8% CoO

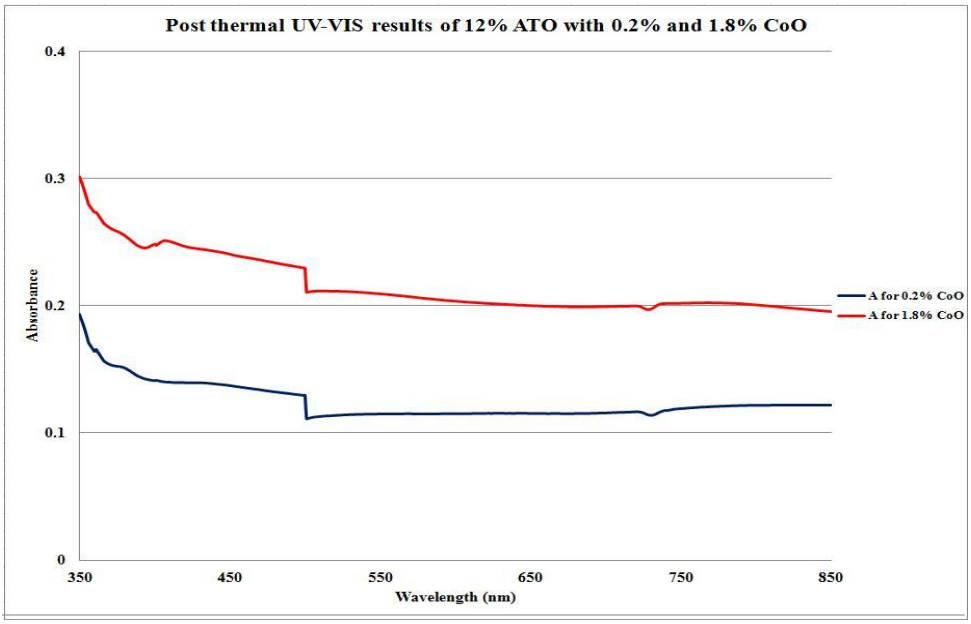

Figure 29: Post thermal UV-VIS absorption results for 12% ATO with 0.2% and 1.8% CoO

6.4 Summary

After treating the samples of different solution concentrations with 85-degree Celsius temperature for 2 hours, the FTIR and UV-VIS was performed once again to check the impact of temperature.

Performing post thermal FTIR, it can be understood that the absorbance and transmittance depended not only on the concentration of ATO but also on the concentration of CoO. The solutions with the lowest and highest absorbance are 8% ATO with 0.2% CoO and 12% ATO with 1.8% CoO. The solutions with the lowest and highest transmittance are 8% ATO with 1.8% CoO and 12% ATO with 1.8% CoO.

Repeating UV-VIS spectroscopy, this time the band gap increments with the rise in the concentration of ATO, and the overall band gaps decrements with the effect of temperature. The 8%, 10% and 12% ATO concentrated solutions had an absorbance wavelength of 500 nm, 490 nm and 480 nm respectively with band gaps of 2.48 eV, 2.53 eV and 2.58 eV respectively.

7 ELECTROSPINNING PROCESS

7.1 Procedure

The process of applying electric field to spin long chain polymers into nanofibers is known as electrospinning. Figure 30 shows the experimental setup of the electrospinning process. The setup has an AC power supply, collector plate and a syringe pump. The collector plate acts as a base, where the nanofibers are collected. The base is wrapped with aluminum foil, as it is a passive material with high electrical conductivity.

The AC power supply provides a variable voltage between 10 kV to 30 kV. To produce strong electric fields around and between the collector plate and needle, we require high voltages. The positive electrode of the AC power supply is connected to the syringe to help pump the solution out of the needle and the electrode that is neutral is connected to the grounded collector plate.

To begin the electrospinning, the syringe is filled with some solution and placed on the pump. The infusion rate is set to a particular value. When the high voltage is supplied, the solution is pumped out from the needle to form a Taylors cone. When the solution is ejected, it searches for an electrical ground, which according to this setup is the collector plate. Hence, the fibers are formed or collected on the aluminum foil. The path of electric field is the path that is detected by the nanofiber as it travels from the needle of the syringe to the collector plate.

The syringe pump can be programmed to set our choice of infusion rate. Per unit time, the solution of a certain volume ejected is known as the infusion rate. The infusion rate depends

on the diameter of the syringe. The diameter should be set on the syringe pump. Once the desired settings are made, the respective solution is filled into the syringe and is electrospun on the collector plate with the supply of a high voltage. The produced nanofibers are a result solely of the polymer present in the solution as this process evaporates the solvent. To have the solvent evaporate from the solution and electrospin the solution accurately with a strong electric field, the distance between the needle tip and the collector plate should be determined [4-5].

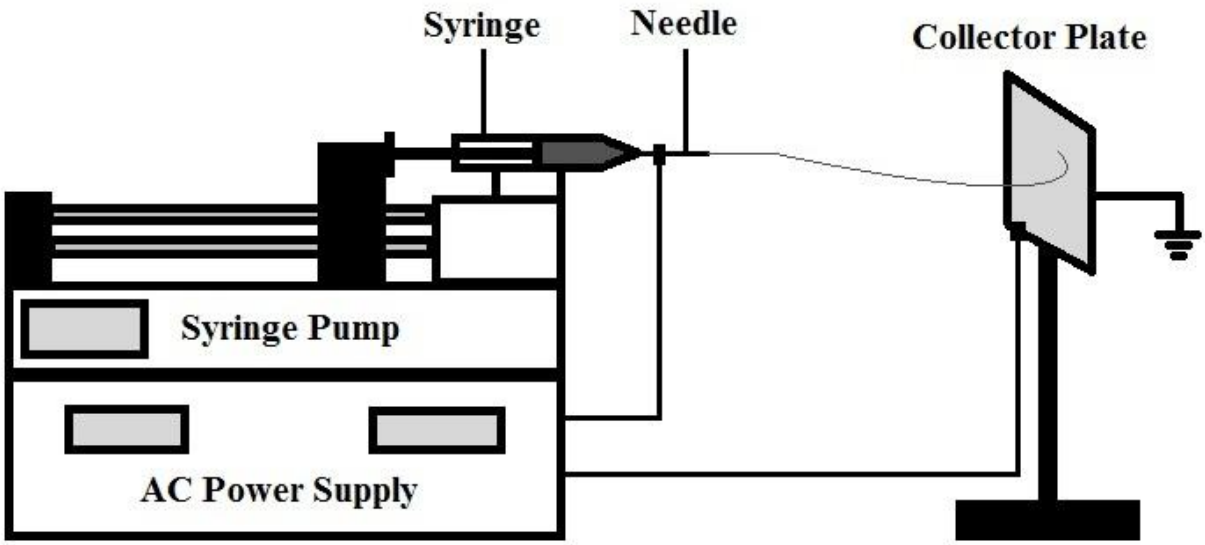

Figure 30: Demonstration of the electrospinning system

7.2 Ideal Parameters

The factors impacting the electrospinning process is the voltage, infusion rate and the distance between the syringe and the collector plate. These factors result in determining the fiber quality and quantity.

High voltages for a range between 10 kilo volts to 30 kilo volts are tried. The voltage of 10 kV corresponded to receiving fewer fibers and the solution ejected from the needle of the syringe and dribbled onto the floor, resulting that the voltage was not high enough to allow the

fibers to reach the collector plate. At a higher voltage of 25-28 kV, the fibers landed on the cabinet wall instead of the collector plate.

As mentioned above, per unit time, the solution of a certain volume ejected is known as the infusion rate. The fibers forming per unit time is less if infusion rate is too slow, thereby it is not reasonable to have low infusion rates. Having very high infusion rates could also be disadvantageous as the solution would drip onto the floor instead of electrospinning, after ejecting from the syringe.

Another important ideal parameter to be considered is the distance between collector plate and needle tip. The collector plate being placed very close to the needle would not form nanofibers and neither placing it too far would help form the fibers. If the collector plate is placed less than 8 inches away from the needle, the solvent from the solution would not evaporate and the mix would be collected onto the collector and then when the succeeding fiber deposits on the preceding one, both would unite to form thin layers of solution instead of forming nanofibers. Ideal distances were found to be 10 and 15 inches.

7.3 Results

Table 8: Ideal parameters of electrospinning process

ATO and CoO (% by weight)	Voltage (in kV)	Infusion Rate (in µL/min)	Distance from the needle (in inches)
8% ATO and 0.2% CoO	15	40	10
8% ATO and 2% CoO	15	40	15
10% ATO and 0.2% CoO	15	40	10
10% ATO and 2% CoO	15	40	15
12% ATO and 0.2% CoO	15	40	10
12% ATO and 2% CoO	15	40	15

For polystyrene as a polymer, the ideal voltage optimized was to be 15 kV. At this voltage, better controlled fibers were formed. Therefore, with a high voltage of 15 kV, 40 µl/min

infusion rate and a distance of 10 inches for 0.2% of CoO and 15 inches for 2% CoO from the needle tip irrespective of weight % of ATO, fibers required were obtained. Table 8 shows the ideal parameters required to electrospin CoO-ATO nanofibers.

7.4 Summary

The entire chapter summarizes the procedures and chosen ideal parameters to obtain electro spun nanofibers with the spin coating and electrospinning process.

SEM was performed on the 10% by weight of ATO with 2% CoO electrospun nanofibers to obtain the thickness. The electrospun fibers gave different thickness fibers of 659nm, 1.97 microns and 3.55 microns at a magnification of 2000. Figure 31 shows the electrospun fibers of 10% ATO and 2% CoO.

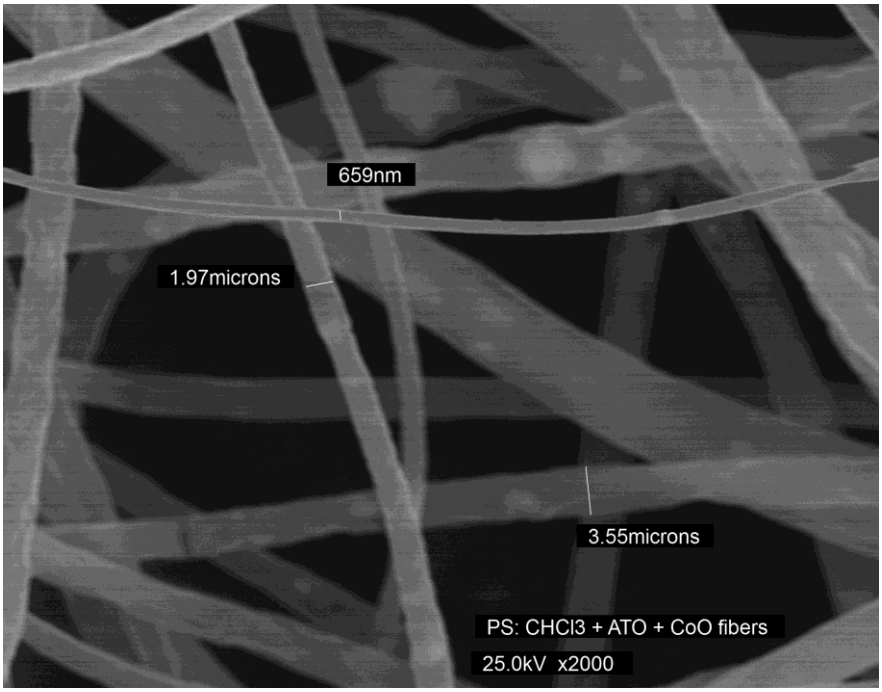

Figure 31: SEM picture of electrospun fibers of 10% ATO and 2% CoO

8 CONCLUSION AND FUTURE WORK

8.1 Discussion

From the results of the FTIR absorption and transmission graphs before thermal treatment, it is inferred that absorbance cannot be more than 100%, which indirectly means that the solution is not dilute enough to allow light to be absorbed. It can be said that with the increase in concentration of ATO, the absorbance decreased and transmittance increased. With the increase in concentration of CoO, absorbance increased and transmittance decreased. The sample with the least absorbance and highest transmittance was the solution with 12% ATO and 0.2% CoO. Similarly, the sample with the highest absorbance and least transmittance was the solution with 8% ATO and 1.8% CoO. From the UV-VIS experimentation, the average band gap was found to be 3.11 eV.

From the results of the post thermal FTIR absorption and transmission graphs, it is discussed that the concentration of both ATO and CoO helped increase or decrease the transmittance and absorbance. The lowest concentrations of both ATO and CoO gave the lowest absorbance and vice versa. The highest concentration of CoO with the lowest and highest concentration of ATO gave the lowest and highest transmittance. The UV-VIS saw a decrease in the absorbance wavelength with the increase in the concentration of ATO and overall there was a decrease in the band gap as well. The average band gap was calculated to be 2.53 eV. The band gap of ATO was 4.62 eV [36] and ranged between 1.6 eV to 3.79 eV for different concentrations of CoO [37].

Another important property noticed is that the energy band gap can be tunable based on the amount of heat treatment and weight concentrations of ATO and CoO.

8.2 Conclusion

With a solar cell technology perspective, we know that reflection and transmission properties of any material are considered to be a loss as the photons cannot be absorbed. The lost photons are a reason to cause electrons to get excited from valence to conduction band. However, as it is discussed in the beginning that the infrared spectrum of light is not converting into electricity and instead causing heat to the solar cell, therefore, using CoO-ATO can help reflect the infrared wavelengths of 8000 nm to 13000 nm.

With the experimentations performed, we can conclude that ATO is indeed a very good anti-reflecting coating and the properties of reflecting the infrared light enhances with the addition of Cobalt oxide as a metal oxide.

8.3 Future Work

In future, determining if the thin film layer or nanofibers can be used as a top or intermediate layer on fabricating a solar cell would help understand the characterization and nature of the material.

The conductivity, sheet resistance and I-V characteristics can be further investigated to calculate the total output power, fill factor and efficiency. Also, XRD can be performed to find the different compositions in the material. Investigating if CoO-ATO can absorb diffused light can also be determined. Apart from the alternative energy industry, this material coating can be tested in various applications such as military and aerospace vehicles to eliminate the infrared light.

REFERENCES

[1] Niranjan, R. S., Hwang, Y., K., Kim, D. K., Jhung, S. H., Chang, S. J., Mulla, I. S., Mater. Chem. Phys., 92(2005), p. 385.

[2] Saadaddin, I, Pequenard, B., Manaud, J. P., Decourt, R., Labrugere, C., Applied Surface Sciences, 253(2007), p. 5240.

[3] Filho, F. M., Simoes, A. Z., Ries, A., Souza, E. C., Perazolli, L., Cilence, M., Longo, E., Varela, J. A, Ceramics International., 31(2005), p. 399

[4] A. F. Spivak, "Electrohydrodynamics of electrospinning process," Ph.D., The University of Nebraska - Lincoln, United States -- Nebraska, 2000.

[5] B. M. Eick, "Electrospinning of ceramic nanofibers," Ph.D., Purdue University, United States -- Indiana, 2008.

[6] Y. Pais, "Fabrication and Characterization of Electrospun Cactus Mucilage Nanofibers," M.S.E.E., University of South Florida, United States -- Florida, 2011.

[7] mediactiu.com, "Master Series," Fungilab. [Online]. Available: http://www.fungilab.com/products/rotational-viscometers/master-series. [Accessed: 06-Oct-2014].

[8] D. Micheli, C. Apollo, R. Pastore, R. BuenoMorles, S. Laurenzi, and M. Marchetti, "Nanostructured composite materials for electromagnetic interference shielding applications," ActaAstronautica, vol. 69, no. 9–10, pp. 747–757, Nov. 2011.

[9] A. Gupta, M. Cizmecioglu, D. Coulter, R. H. Liang, A. Yavrouian, F. D. Tsay, and J. Moacanin, "The mechanism of cure of tetraglycidyldiaminodiphenyl methane with diaminodiphenylsulfone," J. Appl. Polym. Sci., vol. 28, no. 3, pp. 1011–1024, Mar. 1983.

[10] B. D. Richard, "Thermal Infrared Reflective Metal Oxide Sol-Gel Coatings for Carbon Fiber Reinforced Composite Structures," Ph.D., University of South Florida, United States -- Florida, 2013.

[11] E. D. Boland, "Novel apparatus to control electrospinning fiber orientation for the production of tissue engineering scaffolds," Ph.D., Virginia Commonwealth University, United States -- Virginia, 2004.

[12] Frischknecht R., Jungbluth N., Althaus H.-J., Bauer C., Doka G., Dones R., Hischier, R., Hellweg S., Humbert S., Köllner T., Loerincik Y., Margni M. and Nemecek T. (2007) Implementation of Life Cycle Impact Assessment Methods. Ecoinvent report No. 3, v2.0. Swiss Centre for Life Cycle Inventories, Dübendorf, 2007.

[13] Olivier Jolliet, Manuele Margni, Raphaël Charles, Sébastien Humbert, Jérôme Payet, Gerald Rebitzer, Ralph Rosenbaum, "IMPACT 2002+: A new life cycle impact assessment methodology", The International Journal of Life Cycle Assessment, Volume 8, Issue 6, pp 324-330, 2003.

[14] Manopriya Devisetty Subramanyam, Sylvia W. Thomas, Nirmita Roy and Ridita Rahman Khan, "Investigations of CoO-ATO Coatings for Silicon Solar Cells", IEEE Nano 2017.

[15] N. Naghavi et all. Solid State Ionics 156 (2003) 463– 474.

[16] Roy G. Gordon, MRS Bulletin August (2000) 52-57

[17] S. Shanthi et all.; Cryst. Res. Technol. 34 (1999) 8 1037–1046

[18] S. Ngamsinlapasathian et all. Solar Energy Materials & Solar Cells 90 (2006) 2129–2140

[19] Chambouleyron et all.; Solar Energy Materials 1 (1979) 299-311

[20] H.S. Varol et All.; Solar Energy Materials and Solar Cells 40 (1996) 273-283

[21] M. Devisetty Subramanyam, "Fabrication and Comparison of Electrospun Cobalt Oxide Antimony Doped Tin Oxide (CoO-ATO) Nanofibers made with PS: D-limonene and PS: Toluene", University of South Florida, Thesis – 2014

[22] Dr.V.K.Sethi, Dr. Mukesh Pandey, and Ms. Priti Shukla, "Use of Nanotechnology in Solar PV Cell", International Journal of Chemical Engineering and Applications, Vol. 2, No. 2, April 2011.

[23] Nader Nabhani, and Milad Emami, "Nanotechnology and its Applications in Solar Cells", International Conference on Mechanical and Industrial Engineering (ICMIE'2013) August 28-29, 2013 Penang (Malaysia)

[24] Lipi Mohanty, Stephen K. Wittkopf, "Effect of diffusion of light on thin-film photovoltaic laminates", Results in Physics 6 (2016) 61–66.

[25] Kasap, Safa O. *Optoelectronics and Photonics Principles and Practices*, New Jersey: Prentice Hall, 2001. Print.

[26] Bhalchandra V. Chikate, Y.A. Sadawarte, "The Factors Affecting the Performance of Solar Cell", International Conference on Quality Up-gradation in Engineering, Science and Technology (ICQUEST2015), International Journal of Computer Applications (0975 – 8887)

[27] W.E. Kleinjan, J.C.M. Brokken-Zijp, R. van de Belt, J. Loos, K. Lu, and G. de With, "Antimony-doped tin oxide nanoparticles for conductive polymer nanocomposites", Kriya Materials, TU/e

[28] E Sivasenthil and V Senthil Kumar, "Structural properties of tin oxide thin films prepared by sol-gel technique", International Journal of Applied Research 2016; 2(8): 168-171

[29] Iranildes Daniel Santos, Sinara Borborema Gabriel, Júlio Carlos Afonso, Achilles Junqueira Bourdot Dutra, “Preparation and Characterization of Ti/SnO2-Sb Electrode by Pechini’s Method for Phenol Oxidation”, Materials Research. 2011; 14(3): 408-416

[30] Mahendra Kumar Trivedi, Rama Mohan Tallapragada1, Alice Branton, Dahryn Trivedi, Gopal Nayak, Omprakash Latiyal, Snehasis Jana, “The Potential Impact of Biofield Energy Treatment on the Atomic and Physical Properties of Antimony Tin Oxide Nanopowder”, American Journal of Optics and Photonics, 2015; 3(6): 123-128

[31] Hung-Kuan Lin, Chen-Bin Wang, Hui-Chi Chiu, and Shu-Hua Chien, “In situ FTIR study of cobalt oxides for the oxidation of carbon monoxide”, Catalysis Letters Vol. 86, Nos. 1–3, March 2003 (# 2003) 63

[32] M. Th.Makhlouf, B. M. Abu-Zied, and T. H. Mansoure, “Direct Fabrication of Cobalt Oxide Nanoparticles Employing Sucrose as a Combustion Fuel”, Hindawi Publishing Corporation, Journal of Nanoparticles, Volume 2013, Article ID 384350, 7 pages

[33] Devadatha D, Raveendran R (2013), “Structural and Dielectric Characterization of Nickel-Cobalt Oxide Nanocomposite.” J Material Sci Eng S11:003. doi:10.4172/2169-0022.S11-003

[34] Harish Kumar, Poonam Sangwan1, Manisha, “Synthesis and Characterization of Cobalt Oxide Nanoparticles by Sol-Gel Method”, Advances in Applied Physical and Chemical Sciences-A Sustainable Approach - ISBN: 978-93-83083-72-5

[35] M. Lenglet, J. Lopitaux, L. Terrier, P. Chartier, J.E Koenig, P. Nkeng and G. Poillerat, “Initial stages of cobalt oxidation by FTIR spectroscopy”, JOURNAL DE PHYSIQUE IV Colloque C9, supplkment au Journal de Physique 111, Volume 3, decembre 1993

[36] B.C. Yadav, Rama Singh, Satyendra Singh, Ritesh Kumar and Richa Srivastava, "Nanostructured antimony tin oxide synthesized via chemical precipitation method: its characterization and application in humidity sensing"

[37] Nasser A. M. Barakat, Myung Seob Khil, Faheem A. Sheikh, and Hak Yong Kim, "Synthesis and Optical Properties of Two Cobalt Oxides (CoO and Co3O4) Nanofibers Produced by Electrospinning Process", J. Phys. Chem. C 2008, 112, 12225–12233

[38] Babar, A.R., et al., Sensing properties of sprayed antimony doped tin oxide thin films: Solution molarity. Journal of Alloys and Compounds, 2011. 509(6): p. 3108-3115.

[39] Benrabah, B., et al., Impedance studies of Sb doped SnO2 thin film prepared by sol gel process. Superlattices and Microstructures, 2011. 50(6): p. 591-600.

[40] Carlesi Jara, C., et al., Improving the stability of Sb doped Sn oxides electrode thermally synthesized by using an acid ionic liquid as solvent. Chemical Engineering Journal, 2011. 171(3): p. 1253-1262.

[41] Castro, M.R.S., P.W. Oliveira, and H.K. Schmidt, Enhanced mechanical and electrical properties of antimony-doped tin oxide coatings. Semiconductor Science and Technology, 2008. 23(3): p. 035013.

[42] Dua, L.K., et al., Study of spin coated high antimony content Sn–Sb oxide films on silica glass. Materials Characterization, 2008. 59(5): p. 578-586.

[43] Biswas, P.K., et al., Effects of tin on IR reflectivity, thermal emissivity, Hall mobility and plasma wavelength of sol–gel indium tin oxide films on glass. Materials Letters, 2003. 57(15): p. 2326-2332.

[44] Senguttuvan, T.D. and L.K. Malhotra, Sol gel deposition of pure and antimony doped tin dioxide thin films by non alkoxide precursors. Thin Solid Films, 1996. 289(1–2): p. 22-28.

[45] Shanthi, S., C. Subramanian, and P. Ramasamy, Growth and characterization of antimony doped tin oxide thin films. Journal of Crystal Growth, 1999. 197(4): p. 858-864.

[46] Zhu, Y.C. and J.S. Jiang, Synthesis and characterization of alpha-fe2o3@ato nanocomposite particles. Surface Review and Letters, 2008. 15(5): p. 545-550.

[47] Lussier, A., et al., Comparative x-ray absorption spectroscopy study of Co-doped SnO[sub 2] and TiO[sub 2]. Journal of Applied Physics, 2004. 95(11): p. 7190- 7191.

[48] Chen, X.C., Synthesis and characterization of ATO/SiO2 nanocomposite coating obtained by sol-gel method. Materials Letters, 2005. 59(10): p. 1239-1242.